A Summary of Aluminum Combustion*

M.W. Beckstead

Brigham Young University

Provo, Utah, USA

Abstract

The combustion characteristics of aluminum combustion are summarised in an overview of the subject, focusing on the burning time of individual particles. The fundamental concepts that control aluminum combustion are discussed starting with a discussion of the "D^n" law. Combustion data from over ten different sources with almost 400 datum points have been cataloged and correlated. Available models have also been used to evaluate combustion trends with key environmental parameters. The exponent is shown to be less than two, with nominal values of ~1.5 to 1.8 being typical. The effect of oxidizer is pronounced with oxygen being twice as effective as water and about five times more effective than carbon dioxide. The observed effect of pressure and initial temperature is minimal.

In the second part of the paper a two-dimensional unsteady state kinetic-diffusion-vaporization controlled numerical model for aluminum particle combustion is presented. The model solves the conservation equations, while accounting for the species generation and destruction with a 15 reaction kinetic mechanism. Two of the major phenomena that differentiate aluminum combustion from hydrocarbon droplet combustion, namely the condensation of the aluminum oxide product and the subsequent deposition of part of the condensed oxide, are accounted for in detail with a sub-model for each phenomenon. The effect of the oxide cap in the distortion of the profiles around the particle has been included in the model. The results obtained from the model, which include two-dimensional species and temperature profiles, are analyzed and compared with experimental data. The combustion process is found to approach a diffusion controlled process for the oxidizers and conditions treated. The flame zone location and thickness is found to vary with oxidizer. The result shows that the exponent of the particle diameter dependence of burning time is not a constant and changes from about 1.2 for larger diameter particles to 1.9 for smaller diameter particles. Due to the deposition of the aluminum oxide on the particle surface, particle velocity oscillates. The effect of pressure is analyzed for a few oxidizers.

Introduction

Aluminum has been added to propellants for many years as an extra energy source for the propellant. Thus, research on the combustion mechanism of burning aluminum has been an ongoing effort. A very significant effort was expended in the 1960's and 1970's shortly after the effects of aluminum were first conceived. In an early study Glassman[1,2] recognized that metal combustion would be analogous to droplet combustion, and that the D^2 law ought to apply, and that ignition and combustion ought to depend on the melting and boiling points of the metal and the oxide. He speculated that ignition would not occur until the oxide shell melted at its melting point and that subsequent combustion would achieve a steady state condition with the aluminum at its boiling point. These basic concepts have provided a general framework for interpreting aluminum combustion.

* This work was sponsored partly by Brigham Young University and partly by an ONR sponsored Multidisciplinary University Research Initiative under ONR Grant No. N00014-95-1-1338, Program Manager Dr. Judah Goldwasser

Paper presented at the RTO/VKI Special Course on "Internal Aerodynamics in Solid Rocket Propulsion", held in Rhode-Saint-Genèse, Belgium, 27-31 May 2002, and published in RTO-EN-023.

Report Documentation Page

Form Approved
OMB No. 0704-0188

1. REPORT DATE	2. REPORT TYPE	3. DATES COVERED
00 JAN 2004	**N/A**	**-**

4. TITLE AND SUBTITLE	5a. CONTRACT NUMBER
A Summary of Aluminum Combustion	5b. GRANT NUMBER
	5c. PROGRAM ELEMENT NUMBER
6. AUTHOR(S)	5d. PROJECT NUMBER
	5e. TASK NUMBER
	5f. WORK UNIT NUMBER
7. PERFORMING ORGANIZATION NAME(S) AND ADDRESS(ES) **Brigham Young University Provo, Utah, USA**	8. PERFORMING ORGANIZATION REPORT NUMBER
9. SPONSORING/MONITORING AGENCY NAME(S) AND ADDRESS(ES)	10. SPONSOR/MONITOR'S ACRONYM(S)
	11. SPONSOR/MONITOR'S REPORT NUMBER(S)

12. DISTRIBUTION/AVAILABILITY STATEMENT
Approved for public release, distribution unlimited

13. SUPPLEMENTARY NOTES
See also ADM001656., The original document contains color images.

14. ABSTRACT

15. SUBJECT TERMS

16. SECURITY CLASSIFICATION OF:			17. LIMITATION OF ABSTRACT	18. NUMBER OF PAGES	19a. NAME OF RESPONSIBLE PERSON
a. REPORT	b. ABSTRACT	c. THIS PAGE			
unclassified	**unclassified**	**unclassified**	**UU**	**46**	

Standard Form 298 (Rev. 8-98)
Prescribed by ANSI Std Z39-18

A question that has often been asked, is whether laboratory data in air at ambient pressure and temperature can be related to motor conditions at high temperature, high pressure and in propellant products that do not contain oxygen. One of the purposes of this study was to develop sufficient understanding of aluminum combustion based on laboratory data, simulated motor data and actual motor data, to answer that question. Other questions can be asked about the effect of aluminum on combustion efficiency, slag formation, effects of agglomeration, and the potential effect of aluminum on a propellant's burning rate. These questions will not be addressed in this paper, although the understanding gained here should be applicable to some of the questions.

In the 70's and early 80's several survey papers and reports were written, summarizing the work up to that time. Some of the most useful are the works of Pokhil, et al[3], Frolov, et al[4], Micheli and Schmidt[5], Glassman, et al[6], and Price, et al[7,8]. This paper will focus on the burning time of aluminum and the effect of various parameters on that burning time. Extensive research has been performed in Russia (then, the Soviet Union) and brief summary of that work is included. Following that, data from those sources that were available to the author, evaluating the effects of particle diameter, oxidizing species, pressure, and temperature on aluminum combustion.

Aluminum combustion in air[1] suggests that it burns as a vapor and the combustion is controlled by the diffusion of the fuel and oxidizer. However, aluminum combustion cannot be analyzed with a simple hydrocarbon droplet combustion model. This is due to some complications with aluminum combustion. First, in aluminum combustion, the gas phase combustion products condense to liquid aluminum oxide. This condensation dominates the combustion process and contributes considerably to the amount of heat released during combustion. Second, condensed aluminum oxide can deposit on the particle surface to form an oxide cap, which distorts the distribution of gasification velocity, temperature and other quantities around the particle. Also, the oxide cap cam cause jetting and fragmentation of the particle. Third, the dissociation of the condensed product maintains the flame temperature fairly constant at the gasification temperature of the aluminum oxide. Hence, hydrocarbon droplet combustion models cannot be extended directly to model aluminum combustion.

The second part of this paper focuses on modeling the basic combustion process of a burning aluminum particle. Aluminum combustion models have been developed since the 1960's. Brzustowski and Glassman[2] were among the first to suggest that aluminum burns in the vapor phase. They stated that a metal would burn in the vapor phase if its boiling point temperature were lower than that of its oxide. Their model included many of the same assumptions as in hydrocarbon droplet combustion models. Law[3] was the first to acknowledge some of the effects of the oxide condensation in a model. Law's analytical model has been upgraded by Turns[4], Brooks[5,6] and Bhatia[7] by relaxing certain assumptions in Law's model. Many of the earlier models[2,3] have focused on calculating the burning time and flame temperature, but could not predict the distributions of physical quantities nor processes such as condensation and deposition. The postulated combustion mechanisms were much simplified, using global kinetics. Many of the models[2,3,8] have not accounted for the effects of the oxide cap in the distortion of the symmetrical flame. Many of the models have assumed quasi-steady state[3,8,9]. Many of the models have concentrated on aluminum combustion in air, while one of the main uses of aluminum is in rocket motors, where the oxidizers mainly consists of CO_2 and H_2O.

Aluminum Combustion Research in Russia

Overviews and surveys of Russian work on aluminum combustion or metal combustion in general has been performed by Pressley[9] in the US, as well as the Pokhil[3], and Frolov[4], papers previously referenced. The reader is referred to these reports for discussions on the work prior to that time.

In 1968 Belyaev, et al[10] published a classic paper on aluminum combustion, which has been referenced by most subsequent papers in the Russian literature. They incorporated aluminum into propellants at 0.01% so they were measuring the burning rates of individual particles, avoiding agglomeration effects.

They varied the effective CO_2 and H_2O concentrations in the gas, (i.e. a_K), diameter and pressure, and developed an expression for particle burning time as:

$$\tau = 0.67\ D^{1.5}/a_K{}^{0.9} \qquad (1)$$

where D is the particle diameter in μm, a_K is the relative concentration of CO_2 and H_2O in the gas, and τ is the burning time in msec. CO was not considered an active oxidizer because the energy to break down the CO molecule is double that of either CO_2 or H_2O. Below pressures of ~25-30 atm, they observed burning time decreasing ~10-12%, but at greater pressures they did not observe a change with pressure. They varied the propellant formulation so that a_K was varied from 0.3 to 0.7, and particle diameters were varied from 70 to 140 μm, determining the exponent of 0.9, and the coefficient of 0.67 in the equation. They also observed that burning time decreases with increasing ambient temperature up to ~2000K. They examined the ignition time of the particles, concluding that it is proportional to D^2 with an activation energy of ~32 kcal/mol. Equation (1) is the expression used in most Russian papers to describe the burning time of aluminum up to the current time.

Boreisho, et al[11] reported that the photographically determined flame sizes around a burning particle could be 1.5 up to 4 times larger than actual. Arkhipov, et al[12] measured flame distances by dropping burning particles onto glass slides observing flame distances of ~ $3D_o$. Dreizen and Trunov[13] have recently reported similar experiments.

A number of papers have focused on the ignition process of metals, aluminum in particular. Merzhanov, et al[14] postulated that the ignition temperature coincides with the melting point of AL_2O_3, 2300 K, and estimated an activation energy of 17 (Belyaev reported a value of 32). Breiter, et al[15] published an extensive summary of the ignition of metals considering thirteen different metals and six alloys based on Glassman's work in this country. They classified the ignition characteristics of the metals according to the relative densities of the metal versus that of the oxide and the melting point of the oxide. Thus, the impervious character of aluminum oxide inhibits ignition up to the temperature, at which it melts, which then results in ignition and combustion. Ermakov, et al[16] embedded a thermocouple into an aluminum particle, and measured ignition temperatures of ~2000-2100 K, concluding that ignition occurs due to the failure of the oxide shell integrity, but not necessarily due to melting. Lokenbakh, et al[17] contend that mechanical cracking of the oxide shell can occur under varying heating and ambient conditions, leading to ignition and/or enhanced agglomeration at temperatures as low as 1000 to 1300 K. Boiko, et al[18] examined ignition of several metals in a reflected shock wave, also concluding that ignition can occur due to fracturing of the oxide shell when subjected to mechanical stresses. Rozenband and Vaganova[19] also propose ignition by fracture of the oxide shell due to mechanical stresses caused by thermal expansion and density differences during rapid heating. Rozenband, et al[20] also claim that $CrCl_3$ can react with the oxide shell reducing the ignition temperature to ~900K.

The characteristics of the oxide particles formed from the combustion of a metal are very important relative to performance (i.e. combustion efficiency) and acoustic particle damping. Fedorov, et al[21] measured a bimodal distribution of Al_2O_3 in the exhaust from small motors, observing most of the oxide as smoke ~1.5 to 2 μm, but with a second larger fraction of particles ~6 μm. They also observed that the percentage of fines increased at higher pressures. Arkhipov et al[12] measured oxide particles of ~1-2 μm at one atm pressure in a laboratory experiment.

There are a large number of papers discussing models that describe the ignition process leading to metal combustion. For example, Gostintev et al[22], Gremyachkin[23], Arutyunyan, et al[24], etc., all developed models describing the ignition of metals, usually aluminum. Gurevich, et al[25], Gremyachkin[23], Gostintev[22], Bezprozvannykh, et al[26], Rozenband and Vaganova[19] and Kovalev[27] all developed models allowing for the growth of protective oxide on the surface, comparing that to another aspect of the

ignition process (e.g. strength of the oxide layer, transient heating, etc.). Both Gremyachkin and Rozenband and Vaganova showed that ignition could occur well below the oxide melting point. Kovalev[27] showed that the ignition time should be proportional to D^2. Medvedev, Fedorov and Fomin[28] conclude that Mg ignites by thermal explosion while Al ignites by a critical ignition temperature (the oxide melting temperature). There is obviously a diversity of opinion, but also the different authors developed their models for different ignition conditions, some considering slow heating, others considering very rapid heating, etc.

Kudryavtsev, et al[29], Gremyachkin, et al.[30,31], etc all developed models for describing the rate of combustion of metals, usually aluminum. Babuk, et al[32] have studied the effect of metal oxide formation on the combustion. Gremyachkin, et al[31] developed a model for the combustion of aluminum particles (droplets) including oxidizer diffusion to the surface and heterogeneous reaction there. They also contend that aluminum can react with the oxide on the surface forming Al_2O which has a high vapor pressure. They account for the effects of O_2, H_2O and CO_2 as oxidizers, concluding that the burning times for CO_2 are twice as long as for water, and that the burning times for water are 1.5 times as long as for oxygen. Kudryavtsev, et al[29] developed a model including the reaction of aluminum and water. Their model shows burning times constant above ~350 psi, but varying at lower pressure (in agreement with experimental data). They say that the low pressure variation is due to the diffusion process being inhibited by the oxide cloud.

Experimental Investigations into Aluminum Particle Combustion

As part of this study, as much data as possible has been accumulated, documented and assembled in a common format. The various sources are listed in Table I, along with a brief summary of the range of test conditions for which they performed their experiments. Only sources have been used where variations in the data were sufficient to show a trend. Many other sources where data have been obtained at a single set of conditions have not been included. A data base of approximately 400 datum points have been compiled and analyzed to evaluate the dependencies of the various parameters on the aluminum burning time. The results of those studies are presented below.

This brief summary is not necessarily comprehensive, but is intended to identify major research contributions, particularly where burning time data were available that could be correlated with other researchers. A brief description of their technique is included along with a discussion of their results and conclusions. For simplicity, research has been separated by the technique used to ignite the aluminum particle: propellant, gas burner, laser, flash, and shock.

Propellant Ignited Aluminum Particles

Using propellant to ignite aluminum particles is obviously advantageous since conditions similar to that of a rocket motor are created. Yet the high temperature, high pressure, and corrosive environment of propellant combustion is difficult to control experimentally.

Table I - Sources of Aluminum Combustion Data

			Ambient T		Gas Concentrations (%)						
Author	Date	Do (µm)	To (K)	P(atm)	H2O	O2	CO2	CO	N2	Ar	HCl
Friedman & Macek[33,34]	1962 -3	15-67	2510	1	17 to 18	5 to 6	12 to 14	0	63 to 65	0	0
Davis[35]	1963	60-96	2200-3200	1-204	.5 to 50	0 to 27	9 to 50	9 to 41	9 to 41	0	0 -21
Macek[36]	1967	32-49	2500	1	0 to 17	8 to 16	13 to 43	0	40 to 58	0	0
Hartman[37]	1971	23-94	3000-3189	25.5	27 to 34	0 to 4	17 to 23	9 to 30	13 to 20	0	0 - 8
Wilson & Williams[38]	1971	24-74	298	2 - 5	0	10 to 30	0	0	70 to 90	90	0
Prentice[39]	1974	250-400	298	1	0 to 3	15 to 75	0 to 50	0	0 to 80	0 - 85	0
Turns and Wong[40,41]	1987	300-760	1809-1827	1	29 to 31	10 to 25	27 to 30	15 to 49	46 to 64	0	0
Roberts, et al[42]	1993	20	2225-2775	85.-34		99			1		
Marion[43,44]	1995	35-40	298	1 - 39	0	21	0	0	79	0	0
Olsen & Beckstead[45]	1996	40-70	3000	1	66 to 89	11 to 16	0 to 18	0	0	0	0
Melcher, et al[46]	1999	106	2300	13-22	41 to 38	0 to 11	12 to 16	9 to 2	10	0	18
Dreizin[47,48]	1999	90,200	298	1		5-100			5-90	0-95	**
Zenin[49,50]	2000	185-500	298	1 - 40	0	0 to 20	0 to 100	0	0 to 80	0 - 80	0

Davis[35] prepared ammonium perchlorate and paraformaldehyde propellants with less than 1% aluminum by mass. These propellant samples were ignited in a 'bomb' apparatus with pressures ranging up to 200 atm. Particle combustion was captured with high-speed cinematography through windows. Using aluminum particles with initial diameters ranging from 53 to 103 µm, Davis found that an exponent of 1.8 for Equation 3.1 fit the data well. Davis also noted that the burning rate increased while the pressure climbed from 20 to 70 atm, but the rate was constant thereafter. Similar to Davis, Friedman and Macek[33] and Macek[36] also created aluminized propellant samples which burned with pressures ranging up to 135 atm. Friedman and Macek noted that hollow oxide spheres were produced when the apparatus was operated at atmospheric pressure.

Hartman[37] performed similar experiments using composite modified, double base propellant which contained three oxidizers: ammonium perchlorate, nitrocellulose, and nitroglycerin. Varying the formulation of this propellant provided a wider range of oxidizer environments in which aluminum particles could burn. Hartman chose particle distributions with mean diameters of 23, 54, and 94 µm and did testing at pressures of 19, 26, and 50 atm. He found a dependence on pressure and oxidizer environment similar to that seen by Davis. Hartman reported his data by using Equation 3.1, but observed a dependence on pressure raised to the 0.4 power.

Krier (Burton, et al[51] and Melcher, et al[52]) has tried two approaches to investigate aluminum particle combustion with an AP/HTPB propellant as an ignition source. Similar to the research just reviewed, Krier aluminized his propellant sample for one approach. Additional oxygen could be introduced into the propellant exhaust products via an injector to increase the oxygen concentration up to 10%. The burning rate was only slightly dependent on the oxygen concentration, but this conclusion may be in error due to poor mixing of the oxygen with the propellant exhaust. Pressure was varied from 13 to 22 atm and the burning rate increased linearly with pressure over this range. For a second approach, an injector delivered a mono-disperse aluminum particle stream to the exhaust products of a non-aluminized AP/HTPB propellant. Using strobed photographic techniques, burning times were 10±2 ms for nominally 68 µm particles which is in general agreement with other published research.

Gas Burner Ignited Aluminum Particles

In experiments where gas burners are used, the aluminum particles are passed through a gaseous flame hot enough to achieve ignition. Propane, carbon monoxide, methane, hydrogen, and cyanogen are some fuels that have been used. Oxygen is the typical oxidizer with nitrogen used as a dilutant. After an aluminum particle ignites, it burns in the exhaust products of the gaseous flame, which includes both water and carbon dioxide as oxidizer species, in addition to any available diatomic oxygen. These studies create an atmosphere that is similar to that in a solid propellant, but allowing the experimentalist greater control over what could be achieved with actual propellants. With a few exceptions, most studies using gas burners to ignite aluminum particles have been performed at atmospheric pressure since controlling a gaseous flame at high pressures is challenging.[45]. Strobe photography and high-speed cinematography are typical tools used to measure particle burning times.

Friedman and Macek[33,34] and Macek[36] provide some of the first reported burning time data for aluminum particle combustion. They ignited small particles (30 to 50 µm) in propane or carbon monoxide flat flame burners. Little difference in burning times was found using either fuel. In both burners, a fine oxide smoke and porous or hollow oxide spheres were formed. These oxide 'bubbles' were more numerous in the exhaust environments containing water. They also saw consistent fragmentation during the vigorous combustion of aluminum particles in oxygen rich environments. Their data suggested an exponent of 1.2 to 1.5 for Equation 3.1.

Bartlett, et al[53] used a methane flame to ignite several different aluminum particle distributions with mean diameters ranging from 15 to 32µm. Hollow oxide spheres were found after particle burnout which were close to the size of the original aluminum particle. The spheres were crushed and examined under a microscope. A porous structure was observed with small specks of metal.

Davis[35] used a carbon monoxide flame to ignite his aluminum particles that were between 53 and 66 µm. In Davis' photographs he was able to discern that the particle's flame front was several diameters larger than the particle and thus had evidence for vapor-phase combustion. Davis also observed porous oxide spheres in the residue collected after combustion. He noted increasing particle fragmentation for any oxygen concentration over 32% by volume. He suggested that the particle burning time was inversely proportional to the oxygen partial pressure. He also concluded that the ambient oxygen concentration was more important to the particle combustion rate than the ambient temperature.

Drew, et al[54,55], Prentice[39] and Price, et al[56] performed a number of aluminum particle combustion experiments, many of them qualitative, but some were quantitative. Their burners used hydrogen, carbon monoxide and cyanogen combined with oxygen. Particles ranged in size from 30 to 400µm. Burning

times were determined using photographic techniques, and combustion morphology was investigated by using microscopes to examine particles quenched during combustion.

Particle spinning, metal vapor jetting, and violent fragmentation were observed in both the hydrogen and carbon monoxide flames. With a hydrogen flame, a smaller flame diameter was observed, possibly due to the higher diffusivity of water as opposed to carbon monoxide. Also large numbers of hollow oxide spheres were formed. In the carbon monoxide flame, few hollow oxide spheres were present, and a noticeable amount of unburned aluminum was present in the exhaust residue. If just 5% hydrogen were added to the carbon monoxide flame, results were similar to the pure hydrogen and oxygen flame. Particles ignited in the cyanogen flame exhibited behavior similar to that seen with a carbon monoxide flame.

Wong and Turns[40,41] added aluminum powder to jet fuel (JP-10) to create slurry droplets with diameters ranging from 500 to 1100 µm. These droplets were suspended on silicon carbide fibers and then suddenly exposed to the hot exhaust gases of a carbon monoxide or methane flame. Upon burnout of the jet fuel, the aluminum would agglomerate forming an aluminum particle with a diameter ranging from 300 to 800 µm. Using high-speed cinematography, they observed that the vapor-phase flame front was smaller for the methane flame, where water would be present, when compared to the 'dry' environment of the carbon monoxide flame. Also eruptions and fragmentation were noted for the 'wet' environment. They found that burning times decreased when the flames were operated fuel lean such that there was excess oxygen in the flame exhaust.

Olsen and Beckstead[45] used a carbon monoxide/hydrogen diffusion flame to ignite aluminum particles one at a time. A photomultiplier tube was used to record the combustion event. Particles, ranging in size from 40 to 80 µm, were meticulously chosen individually under a microscope. Olsen interrupted the combustion of some particles by quenching. Using scanning electron microscopy and X-ray analysis, he was able to examine the combustion morphology of the particles and the formation of porous oxide spheres that were prevalent. Olsen found that his oxidizer concentration (H_2O, CO_2, or O_2) had a strong effect on the particle burning rate. He concluded that the difference in the burning rate exponent among different researchers was as much due to the varied data reduction techniques used as it was due to the diverse physical conditions of each experiment. Olsen also postulated that the burning rate exponent probably changed during the combustion history of a particle—ranging from approximately two at ignition and decreasing towards one at particle burnout. He suggested this burning rate decrease would occur because of the increasing fraction of aluminum oxide covering the molten aluminum sphere.

Foelsche, et al[57] recently used photodiodes to measure the burning time of a small cloud of aluminum powder (approximate diameter of 22 µm) inside a combustion bomb with pressures ranging from 38 to 145 atm. The aluminum particles were injected into the bomb shortly after the ignition of a $H_2/O_2/N_2$ mixture generated high temperatures and pressures. Foelsche found his data compared favorably with that of Davis, but showed a greater pressure dependency.

Laser, Flash, and Shock Ignited Aluminum Particles

By using lasers, flash tubes, or shock waves some researchers have ignited aluminum particles and observed their behavior. Since this ignition method is independent of the ambient environment, the temperature, pressure, oxidizers, and inert species can be varied widely. Wilson and Williams[38] ignited single aluminum particles with a laser in an oxygen/argon atmosphere. They found that dilute amounts of argon suppressed oxide cap formation and particle fragmentation. Without an oxide cap, the particles appeared to burn in accordance with the vapor-phase model suggested by Brzustowski and Glassman[58].

High-speed photography captured the combustion history of the nominally 50 µm particles in a chamber with pressures ranging to 5 atm.

Drew, et al[59] and Prentice, et al[39,60] used lasers to ignite individual particles. In addition, a xenon flash tube was used to ignite small aluminum foil discs. The molten discs formed particles approximately 250 to 400 µm in diameter. These particles were burned in room temperature combinations of CO_2/O_2, N_2/O_2, and Ar/O_2. For some tests, the atmosphere was made 'wet' by introducing water vapor as a second oxidizer. All experiments were performed at atmospheric pressure. Particle combustion history was recorded with high-speed cameras, while the combustion morphology of quenched samples was examined using scanning electron microscopy.

Oxide caps did not form when the environment was argon and oxygen, similar to the observations of Wilson and Williams. When water was introduced, caps did form. At ambient temperature, the particles would extinguish in the carbon dioxide environment before all the aluminum metal was consumed. With an N_2/O_2 atmosphere, the particles would consistently fragment irrespective of the amount of water vapor present. Once again, hollow oxide spheres were observed for many test cases.

Roberts, et al[42] used a shock tube to ignite aluminum, magnesium, and aluminum/magnesium alloy particles at pressures up to 34 atm in almost pure oxygen. Several thousand particles with a nominal diameter of 20 µm were placed on a knife blade near the reflecting wall of the shock tube. The passing shock knocked the particles into free fall and ignited them where a photodiode recorded the light emitted during combustion. The researchers concluded that the burning time for the aluminum particles was not a strong function of pressure although a slight decrease in burning time was noted for increasing pressure.

Bucher, et al[61,62,63] used a 150 W laser to ignite aluminum particles nominally 230 µm in pure N_2O, pure CO_2, and in mixtures of O_2, N_2, Ar, and He. In-situ temperature and species distributions around individual burning particles were made using planar laser-induced fluorescence. Quenched particles were investigated with electron probe microanalysis. Bucher found that the flame diameter around a particle decreased with varying environment gas mixture in the following order: O_2/Ar, O_2/ N_2, CO_2, and N_2O. AlO was found to be an intermediate species in the combustion reaction while for the first time the presence of aluminum-oxy-nitrides was established. Measurements confirmed the idea that the aluminum oxide’s boiling point limits the flame temperature.

Marion, et al[43,44] measured the burning time of 40 micron aluminum at 1 to 40 atm in air, using a laser for ignition. Burning times were observed to decrease slightly with pressure increasing from 1 to 4 MPa. They also report calculated burning times for a modified Law model[64] (very similar to the Brooks[65] model). In calculating the decreasing size of the aluminum particle, they predicted a residual oxide particle approximately 70% of the size of the original aluminum particle, and increasing slightly with increasing pressure. Their predicted burning times are slightly greater than experimentally observed burning times, and they attribute that to the uncertainty in the density-diffusivity product which they used in their model.

Dreizien and Trunov[13] burned 150 µm Al droplets in air at room temperature and 1 atm, similar to Prentice's work. They saw a region of spherically symmetric burning, followed by two regions of oscillating burning with the particles giving off smoke jets and spiraling.. Subsequently Dreizien[47,48] tested 90 and 250 µm particles in N_2/O_2, Ar/O_2, He/O_2 and pure O_2 varying concentrations. He saw spinning and periodic brightness oscillations mainly in the N_2/O_2 case but also in He/O_2. The size of observed oxide caps are much smaller with Ar/O_2 and He/O_2 than in air. He reports burning time data for

the mixtures at varying concentrations, showing a significant decrease in burning time with increasing oxygen concentration. Rates in argon, nitrogen and helium fall virtually on top of each other He assumes this is due to the fact that the density-diffusivity product is approximately constant. He has also examined the aluminum flame structure both with and without gravity, using photomultiplier tubes.

Summary of Experimental Combustion Data

The burning time data from as many of these sources as could be readily determined from their papers are presented in Figure 1. The data scatter is readily apparent. Several of the investigators only used a single particle size, varying the test conditions. For example, Dreizin[47,48] did extensive testing varying gas concentrations, but with only two particle sizes. Melcher[46] and Roberts[42] both did their testing with a single particle size, and much of Prentice's work[39] was done with a single particle size. The differing test conditions lead to different burning times, introducing what appears as "data scatter" in Figure 1. The following sections discuss various other sources of data scatter. It is curious that the optimum fit of the data results in a D^2 correlation. The following sections will also address the potential value of the burning time exponent.

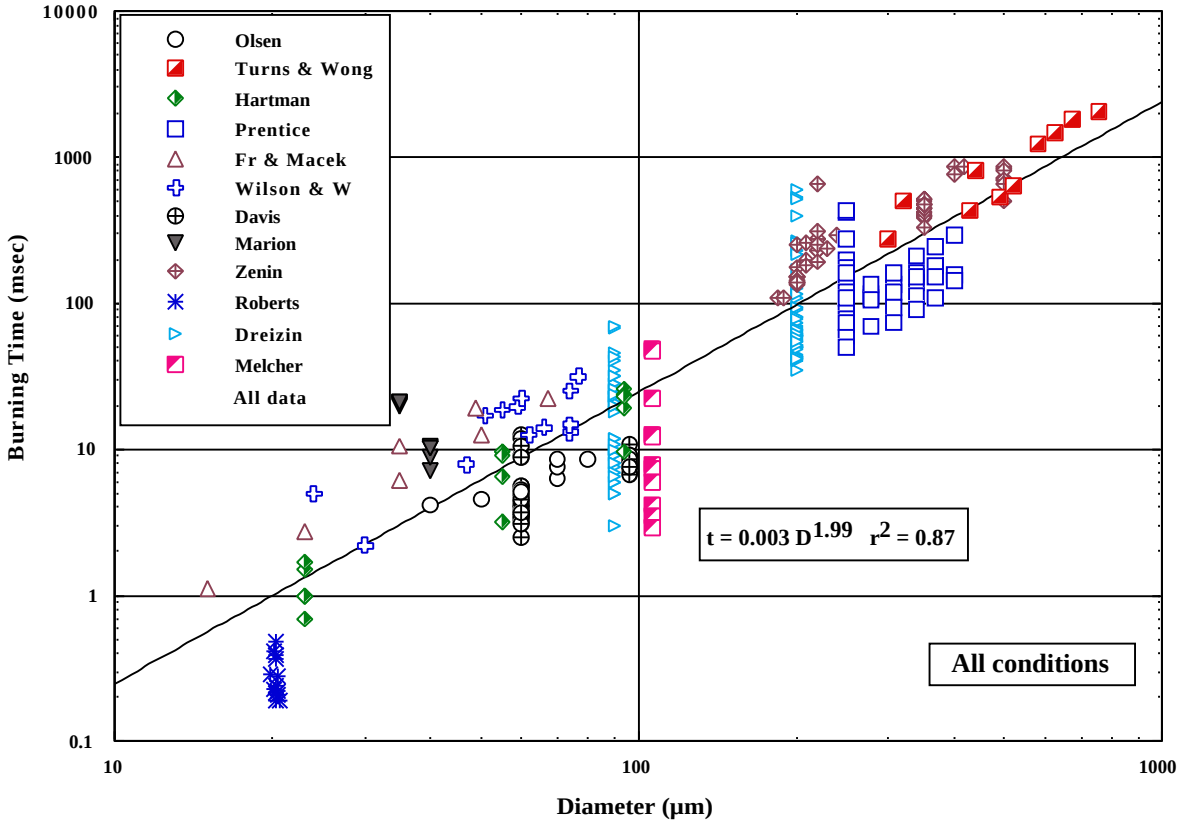

Figure 1. Aluminum burning time measurements from eleven different sources, measured under a wide variety of conditions and test techniques.

The "D^2" Law in Aluminum Combustion

The geometrical aspect of particle or droplet combustion can be described by a simple mass balance. Assuming that the droplet is spherical and regresses uniformly, the mass burning rate will be

$$\dot{m} = -\frac{d}{dt}\left(\text{volume} \times \text{density}\right) = -\frac{d}{dt}\left(\frac{4}{3}\pi r^3 \rho\right) = -4\pi r^2 \rho \frac{dr}{dt} \qquad (2)$$

or, in terms of diameter

$$= -\pi D^2 \rho \frac{d(D/2)}{dt} = -\frac{\pi D \rho}{4}\frac{dD^2}{dt} \qquad (3)$$

Solving for the rate of change of the diameter gives

$$\frac{dD^2}{dt} = -\frac{4\dot{m}}{\pi D \rho} = \text{constant} \qquad D^2 = D_o^2 - \beta t \quad \text{where } \beta = \frac{4\dot{m}}{\pi D \rho} \qquad (4)$$

Solving for time

$$t = \frac{D_o^2 - D^2}{\beta} \qquad \text{at burn out, } D \quad 0 \qquad t = \frac{D_o^2}{\beta} \qquad (5)$$

This is the D^2 law. The question is how well it applies to the combustion of aluminum. First, it should be noted that the inherent assumption is that the spherical droplet is regressing uniformly. Many of the papers discussed above have noted that an oxide lobe develops on the burning aluminum. Thus, the droplet is NOT regressing uniformly. If one accounts for this, the complete spherical surface area is not available for combustion, leading to a reduced exponent in the D^n law. Second, it is assumed that the particle burns out to a diameter of zero. This is not consistent with experimental observations either. Many researchers have observed fragmentation of burning aluminum, indicating that towards the end of burning the residual aluminum/oxide cap can break up in a violent manner, resulting in more than one resultant particle. In addition, even when fragmentation does not occur, the residual oxide particle is often very large, due to porosity. The fact that the particle does not burn to a diameter of zero will also lead to a reduced exponent (less than two). Marion, et al[44] recently used a model to calculate the burning time of aluminum. Within their model they calculate the size of the residual oxide, with fractional values of 0.6 to 0.7 compared to the original aluminum particle.

The conclusion of these observations (including those of many of the above researchers) is that few would expect the exponent to have a value of two. A value of 1.5 to 1.8 is much more likely.

Some of these observations are reinforced by a recent paper by Olsen and Beckstead[45]. A series of tests were performed interrupting the burning process with a glass slide, and then taking SEM photographs of the residual particles. Particles were hand selected to be as close to the same size (70µm) as possible and then were interrupted at increasing distances from their ignition source. Figure 2 is an example. An interesting aspect of this SEM is that the right hand side of the figure is the Al2O3, while the much smaller lobe of the sample is the aluminum. This was determined from the smoke halo on the left and by X-Ray analysis, showing that the oxide cap can be larger than the original aluminum later in burning.

The right hand lobe of the particle is oxide and the left hand, donut shaped part of the particle is aluminum.

As part of the tests, a photodiode was used to register the light intensity from the burning particles. Figure 3 contains the photodiode traces for five different particles quenched at different distances. The particle in Figure 2 was the second trace in Figure 3. It is apparent (see also the full paper by Olsen) that if one uses the entire photodiode trace to determine the burning time of a particle, the majority of that time will represent the combustion of a small fraction of the aluminum. The majority of the aluminum is burned very quickly, but a photodiode will continue to register light, just from the hot, radiating oxide particle, with a very small fraction of aluminum still burning. From examining each of

the five particles, it is evident that a large fraction of the aluminum was burned by the time the first particle was quenched, representing a burning time of ~1.5 msec. If one were to take the entire trace as the burning time a value of 6.5 msec would be recorded. The potential variability in choosing a "burning time" by different researchers can introduce a significant amount of data scatter when comparing data from different sources.

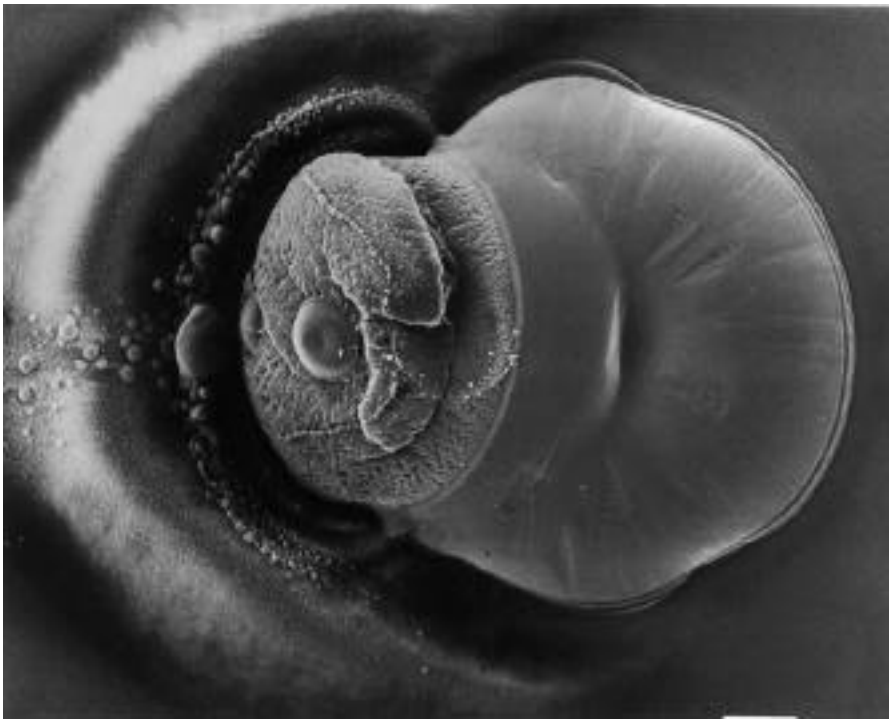

Figure 2. SEM micrograph of a 70 µm aluminum particle quenched 2.5 to 3 msec after ignition.

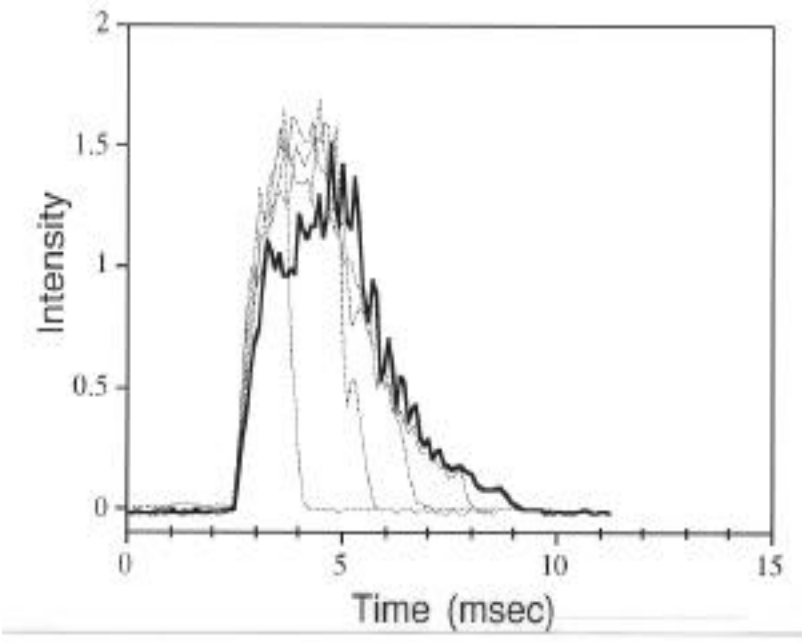

Figure 3. Photodiode emission traces of five different 70 µm aluminum particles quenched on glass slides at varying distances from the ignition point.

In an analytical modeling study[65], the relative amounts of aluminum and oxide were estimated as part of the calculated burning time. Those results are shown in Figure 4 for a 35 µm particle burning in a simulated propellant atmosphere at one atmosphere. Two calculations are reported; one accounting for oxide accumulation on the particle and the other neglecting oxide buildup. The calculation ignoring oxide buildup gives a burning time the correlates with D^2, while the calculation allowing for oxide accumulation gives a $D^{1.5}$ relationship. These results are consistent with those of Marion, previously referenced, and represent another argument that the diameter exponent must be less than two.

In most experimental investigations, the measured aluminum particle combustion has varied from the simple D^2 model. For example, Pokhil, et al[3], Law[66], Prentice[39], King[67], Kuo[68], Brooks[65] and Melcher, et al[46] have all suggested a lower value of the exponent, varying from 2.0 to as small as 1.2. The statistical analysis that has been performed as part of this study indicates that an n of ~1.8 appears to correlate the data best.

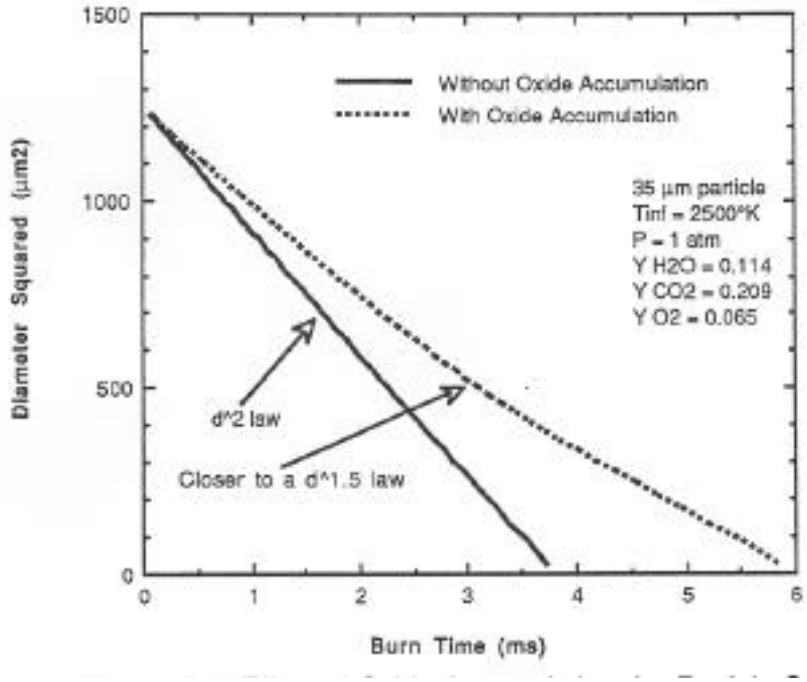

Figure 4. Calculated effect of oxide accumulation on the surface of a burning particle, using the Brooks model[65].

Effects of Oxidizing Atmosphere

The Effect of Oxygen

Referring to the data scatter in Figure 1, it is apparent that much of the scatter is due to the different oxidizing (and inert) gases used in the different tests. Several investigators focused on the effect of the different environmental gases. Prentice performed experiments varying the oxygen content with the other gas being nitrogen or argon. These tests were done at one atmosphere with 250 µm particles. His results are presented in Figure 5. The results show a very pronounced effect of oxygen concentration; the higher the concentration, the shorter the burning time. This is to be expected, because in a diffusion

flame the concentration gradient is the principle driving force for the flame, and higher concentrations should result in shorter burning times.

Prentice also varying the particle diameter along with varying the oxygen concentration. Those results are presented in Figure 6, plotted as burning time versus diameter. The data of Turns and Wong and of Zenin are included for reference, and the overall correlation curve is included also. These results show the same effect as that of Figure 5, but within the context of the usual burning time curve.

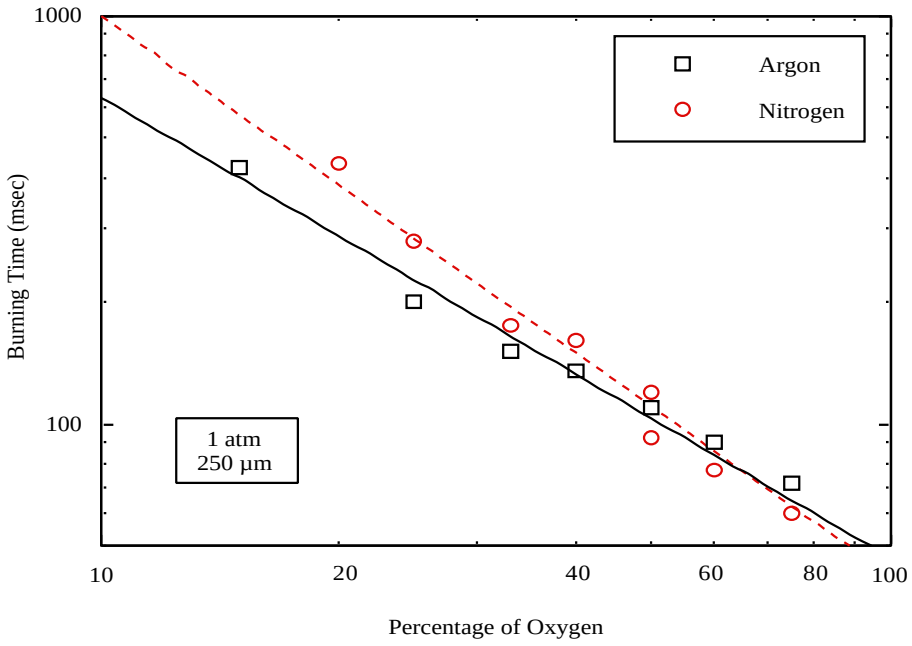

Figure 5. Prentice[39] data for 250 µm particle burning in oxygen/nitrogen and oxygen/argon.

The Effect of Diffusivity

More recently Dreizin[47] has reproduced data very similar to Prentice's, varying the oxygen concentration with inert gases of nitrogen, argon and helium. His results substantiate Prentice's results in a very quantitative manner. Using helium adds another dimension to the data. The differential equation describing diffusion contains the product of diffusivity times density both multiplying the concentration gradient. Thus it is important to consider the potential effect of diffusivity in the combustion process. In general, the diffusivity is proportional to temperature to the 1.65 power and inversely proportional to the pressure. Thus, the product of the density times the diffusivity should be approximately independent of pressure, but slightly dependent on the ambient temperature (approximately the 0.65 power). Helium has a higher diffusivity than nitrogen or argon, but it has a much lower molecular weight (which enters in to the product of density times diffusivity). Thus, the low molecular weight can compensate for a high diffusivity.

Dreizin's data (for 200µm particles) are plotted in Figure 7, comparing them to Prentice's 250 µm data. The data show that the burning time decreases, going from nitrogen to argon to helium, for low concentrations of oxygen. The molecular weight is not in the same order, i.e argon is 40, nitrogen is 28 and helium is four. A similar effect was postulated by Widener[69] in the correlation that he developed. He included the effect of diffusivity, particularly that of hydrogen. He did see a consistent effect,

dependent on the amount of hydrogen produced from the water/aluminum reaction. This observation warrants further invstigation.

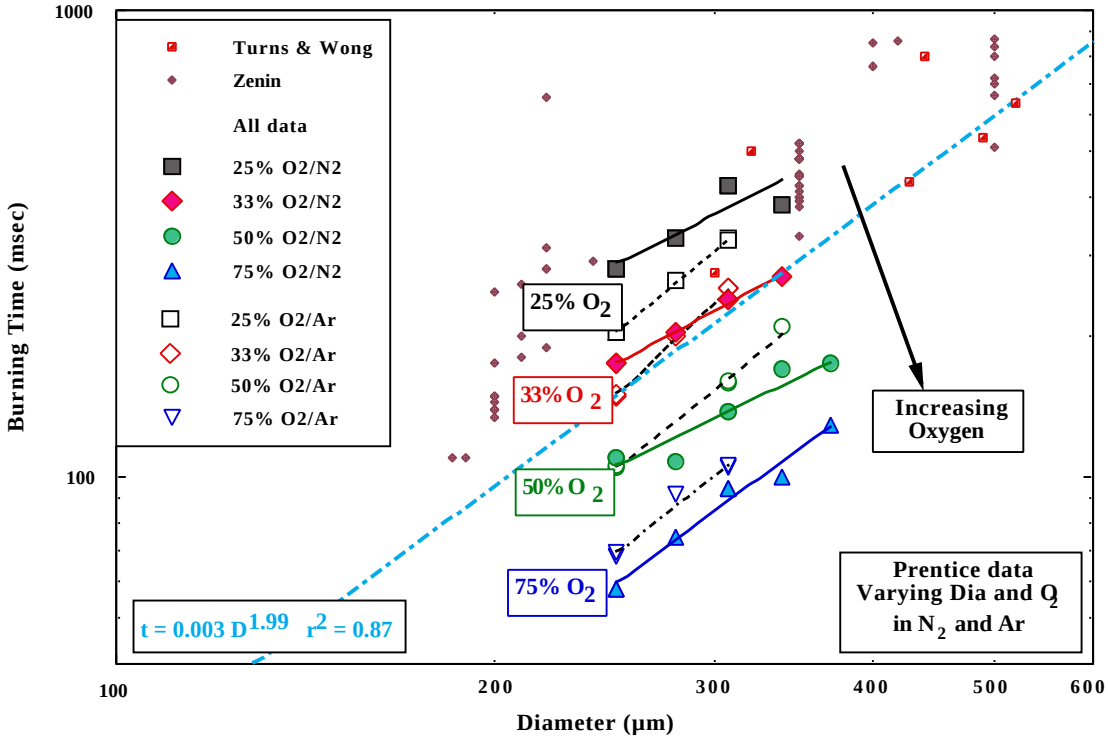

Figure 6. Prentice[39] data varying particle size and burning in oxygen/nitrogen and oxygen/argon.

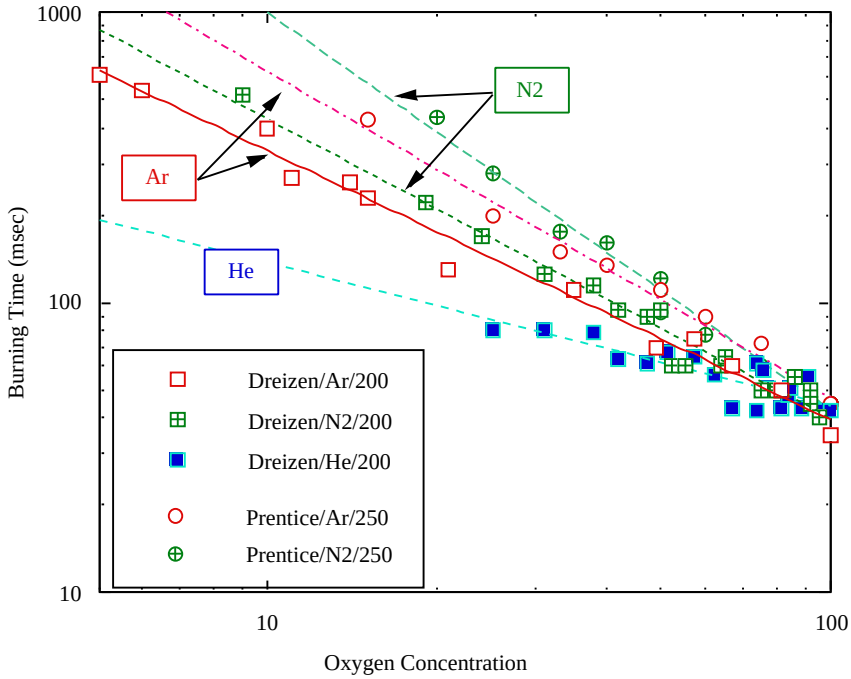

Figure 7. Data from Prentice[39] and Dreizin[47] varying oxygen concentration in nitrogen, argon and helium.

The Effect of CO_2 and Water

Determining the effect of CO_2 and water on the burning time has proven somewhat elusive. It is difficult to create laboratory tests where one can systematically vary the concentrations of CO_2 or water. Most of the data the involve CO_2 and water come from tests involving either propellant or a gaseous flame. Olsen varied the amount of water in his experiments by utilizing a hydrogen flame, giving a greater amount of water than normal. Unfortunately, it was still difficult to make systematic variations in the water content. Thus, the available data are much less definitive than the oxygen data discussed above. In Widener's previous correlation he arrived at relative values for oxygen water and CO_2 of 1:0.58:0.25.

Recently Zenin[49,50] has burned aluminum in air and in CO_2, giving an excellent set of data for determining the influence of CO_2. He also burned the same size particles in mixtures of oxygen/nitrogen and oxygen/argon, similar to Dreizin and Prentice, but not over a range of concentrations. Figure 8 contains his data for 220 and 350 µm particles in 20% oxygen and both nitrogen and argon. He then burned the same size particles in 100% CO_2. The burning times in 100% CO_2 were essentially the same as in 20% O_2. The conclusion is that CO_2 is only ~20% as effective an oxidizer as O_2. The averaged data from Prentice for his 250 µm particles in O_2/argon and Dreizin's 200 µm particles also in O_2/argon are included for reference.

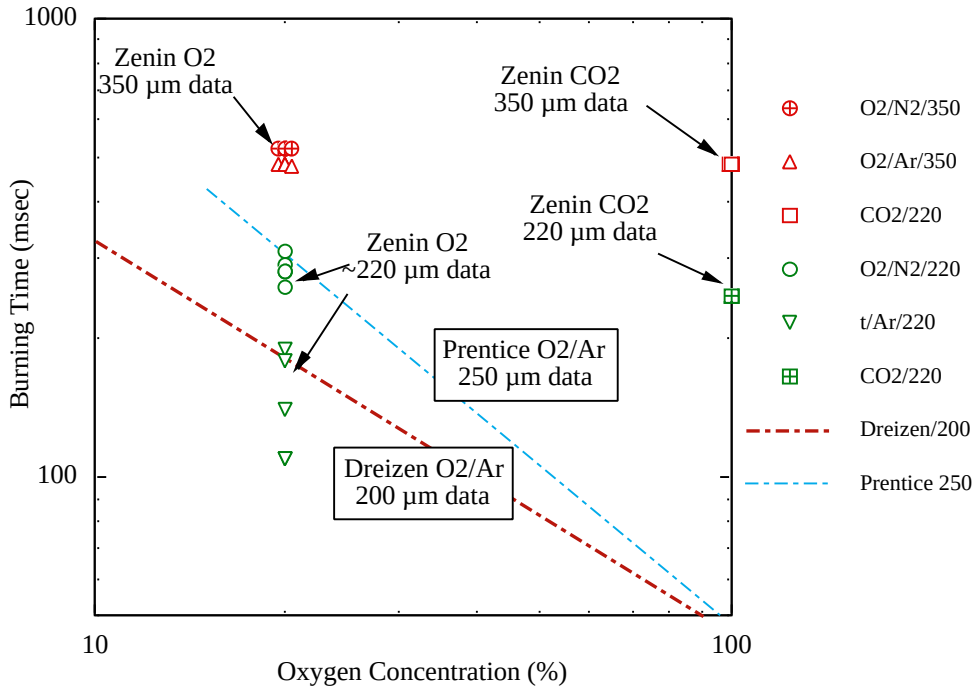

Figure 8. Zenin's data[49] comparing rates for O_2 and CO_2 as oxiziders. Data from Prentice and Dreizin are included for reference (see Figure 7).

From the available data there were no studies that provided data on the effect of water that were conclusive. Brooks[65] suggested defining an effective oxidizer, weighting the relative effects of oxygen, water and CO_2.

$$Xeff = C_{O2} + a_{H2O}\, C_{H2O} + a_{CO2}\, C_{CO2}$$

Using his model calculations in his original publication, he arrived at coefficients of 1:0.533:0.135. The results from various studies are summarised in Table II. Based on the current study, the CO_2 coefficient would appear to be ~0.22. Several different ways of analyzing the data have all led to the same value. This is apparently due to Zenin's data. Because he measured burning times in 100% CO_2, that large percentage apparently weights the data significantly, yielding the coefficient of 0.22. As mentioned above, data varying the concentration of water are very difficult to achieve, and the results there are some what inconclusive. The current study indicates that a value on the order of 0.5 to 0.6 yields relatively consistent results. It is interesting to note that the agreement between the different studies is surprisingly consistent.

Table II - Relative Oxidizer Coefficients for Water and CO_2

	Year	O_2	H_2O	CO_2	Source
Belyaev[10]	1968	-	1	1	Data?
Kudryavtsev[29]	1979	1	0.667	0.333	Model
Brooks[65]	1995	1	0.533	0.135	Model
Widener[69]	1998	1	0.67	0.33	Model
This study	2000	1	0.5-0.6	0.22	Data

Effects of Pressure and Ambient Temperature

Studies on the effect of pressure have also been rather inconclusive. In the early Russian work, it was proposed that the pressure has a small effect at low pressure, but no effect above ~20 atm. This may be a reasonable approximation. The recent work by Marion concludes essentially the same as the early Russian work. Using the effective oxidizer definition with the values noted in the previous section, all of the available data where pressure was a variable were plotted as $t \cdot Xeff/D^n$ versus pressure to determine if there were a trend. The data scatter is still very large, but using a pressure exponent of -0.1, as Belyaev and Marion did, yields the best results. Using the diameter exponent of 1.8 produced a slightly reduced scatter in the data relative to using an exponent of 1.5.

Studies on the effect of initial temperature have also been somewhat inconclusive. Virtually no data exist where some one has systematically varied the initial temperature. The statistical analysis of the entire data set gave a minimum error with the initial temperature exponent of -0.2. Using the diameter exponent of 1.8 produced a slightly increased scatter in the data relative to using an exponent of 1.5.

Summary Correlation of the Data

Based on the analysis of the entire set of data, the following equation is proposed to estimate burning times of aluminum particles:

$$t_b = \frac{a\, D^n}{Xeff\ P^{0.1}\ T_o^{0.2}} \qquad (6)$$

where $X_{eff} = C_{O2} + 0.6\, C_{H2O} + 0.22\, C_{CO2}$

$a = 0.0244$ for $n = 1.5$ and

$a = 0.00735$ for $n = 1.8$

and pressure is in atmospheres, temperature in K, diameter in μm, and time in msec.

The results are shown in Figure 9, where the modified ordinate is $t_b\, X_{eff}\, P^{0.1}\, T_o^{0.2}$.

The raw data from Figure 1 are also re-plotted in Figure 9 to provide a basis of comparison. A regression analysis for the modified data gives an r^2 value of 0.964 while the corresponding regression of the raw data gives an r^2 of 0.87. The reduced data scatter between the correlation and the raw data is readily apparent. The most significant effect contributing to the reduced scatter is the utilization of the effective oxidizer definition. In spite of the reduced scatter, it is somewhat discouraging to see the relatively large data scatter that still exists. This is apparently due to the diversity of methods used to obtain the data, and the different methods of reducing the data, i.e. defining particle burn-out.

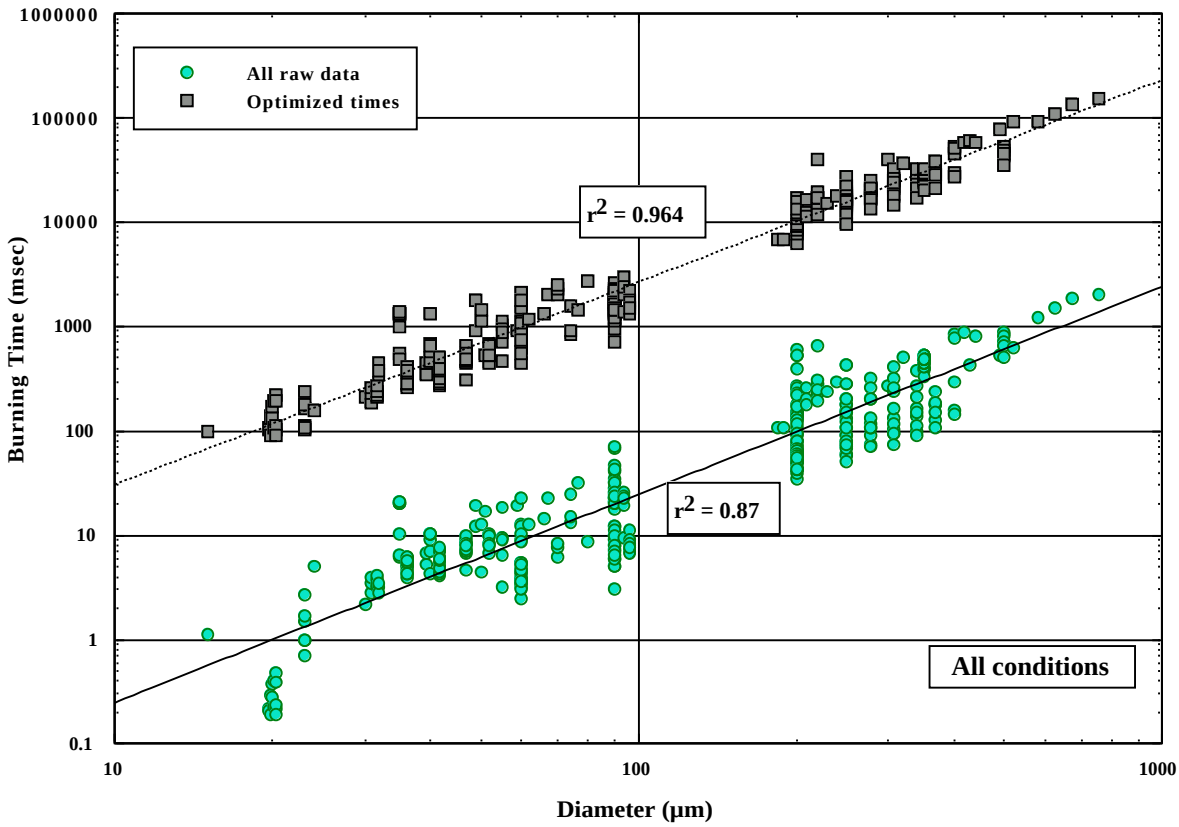

Figure 9. A comparison of aluminum burning time measurements with the proposed correlation of burning times, multiplied by the effective oxidizer and initial temperature and pressure raised to a power.

Modeling Aluminum Combustion

This section of the paper summarizes the modeling work by Liang and Beckstead[69,70,71,72,73,74] simulating aluminum particle combustion at both laboratory and rocket motor conditions.

Background

The adiabatic flame temperature for aluminum combustion is typically greater than the boiling point of aluminum. For example, in the case of aluminum combustion in oxygen at 1 atm, aluminum has a boiling point of 2791˚K, which is below the flame temperature of 4000˚K[1]. The heat feed back from the flame causes the aluminum at the particle surface to vaporize and the vapor proceeds to burn homogeneously in the gas phase with the oxidizer at some distance from the particle surface. There are a few exceptions however, as in the case of aluminum combustion in CO where aluminum burns heterogeneously.[61] Aluminum sub-oxides are the main initial products at the flame zone. The aluminum sub-oxides condense to form liquid aluminum oxide. In the flame zone, the heat release, if sufficient, is used to dissociate the main combustion product, liquid aluminum oxide. Due to the dissociation, the maximum temperature is maintained at the dissociation temperature of the oxide until all the oxide is dissociated. The flame zone position and thickness are both functions of the oxidizer and pressure.

During solid propellants combustion under rocket motor conditions, the embedded aluminum particle is in the molten state on the solid propellant surface due to the heat from combustion of other solid propellant ingredients. Agglomeration of the aluminum particles occurs on the surface of the regressing solid propellant. The agglomerated molten particles at the propellant surface lift off from the propellant surface due to the force of the gases from the propellant surface. The aluminum particles then undergo homogeneous combustion until they reach the nozzle of the rocket motor.

The major product of aluminum combustion is liquid aluminum oxide, which is formed from the condensation of aluminum sub-oxides. A fraction of the oxide diffuses back and deposits on the particle surface and is termed as the ‘oxide cap’. The oxide cap tends to accumulate on the lower end of the falling particle. The accumulation of the oxide on the particle surface and the porosity of the oxide cap result in a final oxide cap size of the order of the initial particle size. The other fraction of the oxide is transported outwards and is termed as the ‘oxide smoke’. The oxide smoke can be seen as a trail of white smoke behind the particle. The oxide smoke dampens the acoustic instabilities in a rocket motor and hence the quantity of smoke formed is important in a rocket motor.

The oxide cap results in fragmentation and jetting. The burn time is proportional to the initial diameter raised to the power of the order of 1 to 2, which is in contrast to the exponent on the diameter being exactly 2 for hydrocarbon droplet combustion[1]. This is apparently due to the formation of the oxide cap, which increases the burn time. The oxide cap effect on the burning time depends on the initial size of the particle too.

Liang and Beckstead’s Model

The model by Liang and Beckstead is a 2-dimensional, unsteady state, evaporation-diffusion-kinetics controlled numerical model. The physical interpretation of the model is depicted in Figure.10. The model simulates the combustion of a single aluminum particle, after ignition, free falling in an atmosphere containing the oxidizer. The model has been developed to describe aluminum combustion in rocket motors. The ignition temperature is typically in the range of 1700°-2200°K. In rocket motors, the aluminum particle usually ignites near the propellant surface. Hence in this model, ignition has been assumed to have occurred initially and the model concentrates on the combustion after the ignition.

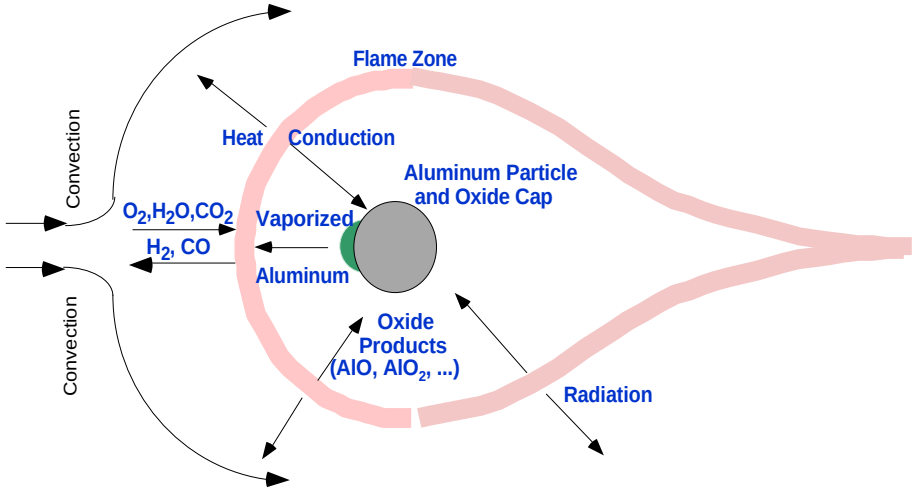

Figure 10. Conceptual schematic of the combustion process surrounding an aluminum particle

For the sake of convenience, gravity is taken to act in the horizontal direction from the right to left direction. The particle falls with some acceleration, after being released from an initial velocity. The acceleration has been taken to be due to gravity for the calculations presented in this paper. Deceleration has been taken to occur due to the drag and the effect of the large flux of aluminum due to evaporation from the particle surface. Since ignition is taken to have occurred, the initial particle surface temperature is taken to be the boiling point of aluminum at the prevailing pressure. A flux of the oxidizer from the surroundings towards the aluminum particle and a flux of aluminum from the particle surface outwards results in the fuel and oxidizer reacting homogeneously to form aluminum sub-oxides and other products in accord with some kinetic mechanisms. The aluminum sub-oxides undergo a reaction followed by homogeneous condensation to form liquid aluminum oxide. Diffusion and convection results in a portion of the condensed aluminum oxide depositing on the particle surface to form an oxide cap. The oxide cap blocks the evaporation of the aluminum from under the region it covers and thus causes a modification in the species and temperature profiles. The oxide cap also provides heat to the evaporation of the aluminum due to the higher temperature of the oxide cap than the particle surface. The heat required for the vaporization of aluminum is provided by the heat feed back from the flame which includes the radiation heat from the flame, heat conduction from gases surrounding the particle and the heat due to the deposition of the oxide cap. The particle radius changes with time due to the vaporization of aluminum and the deposition of oxide cap. The model considers the r and θ directions (in spherical coordinates) and solves the continuity, r and θ momentum, energy and species continuity equations simultaneously to obtain the species and temperature profiles and the burn time. There seems to be no accepted method in the literature for calculating the burn times for aluminum particle combustion. This model estimates the burn time as the time required for the particle to be 95% consumed.

Although experimental results have indicated that the flame zone is within a distance of 10 particle radii, the calculation domain for this model covers 60 particle radii to ensure that the input conditions are totally unaffected by the combustion. Due to convection, all the input of oxidizers from the surroundings to the calculation domain is taken as from the left half of Figure.10 and all the output of gases, including inert and product gases, to the surroundings is taken as from the right half. The symmetricity of the flame is affected by the convection and the oxide cap.

The model is capable of handling different oxidizers, pressures, input enthalpies and accelerations. The transport and thermodynamic properties are calculated using the CHEMKIN transport and thermodynamic package[75], thus relaxing the common assumption of constant physical properties[41,66,67,76]. The transport and thermodynamic properties are calculated for every node for each time step for the various species. The fragmentation and jetting processes have not been considered, since no concrete rationale has been established to describe these processes. By using a numerical model, many of the simplifications required for an analytical model[66,41,76] have been relaxed.

The assumptions made in the model are:

1) The particle is spherical

2) Flow around the particle is laminar

3) The local homogenous flow (LHF) model is applicable to the liquid aluminum oxide smoke.

The flow around an aluminum particle is usually laminar in rocket motor conditions, due to the small size of the particle (typically diameter is less than 200μm). The model had been used initially for investigating air and O_2-Ar at atmospheric pressure, since most of the available experimental data are for those conditions. These data served to validate the model. However, as has been mentioned previously, the typical oxidizer in a rocket motor is CO_2 and H_2O. Hence, the investigation of aluminum combustion with the CO_2-Ar and H_2O-Ar oxidizers, both at atmospheric pressure and higher pressures has been made. It may be noted that the oxidizer in a rocket motor for aluminum combustion consists of a high percentage of CO, but aluminum combustion in CO has not been considered. This is because aluminum burns heterogeneously in CO due to thermodynamic considerations, and since surface reactions are involved, it can be expected that the reaction rate will be slow when compared with the homogeneous gas phase reactions with the other constituents like CO_2 and H_2O. The atmospheric case investigation has been done for the CO_2 and H_2O oxidizers to compare the results with some experimental data pertaining to species and temperature profiles. This has been followed with a study of high pressure combustion in a mixture of gases that resemble the oxidizer in a rocket motor.

Aluminum Combustion Mechanism

Many of the previous models have assumed infinite kinetics.[2,64,65] There has been some question as to whether aluminum combustion is purely diffusion controlled or if kinetics can have an influence.[67,69] Experiments have also shown that the flame zone thickness, which is also an indicator of the pace of the kinetics, varies with each oxidizer.[62,63] In the case of CO as the oxidizer, it has been suggested from experimental data that the combustion could be heterogeneous,[63] which might lead to a kinetically controlled process as surface reactions are expected to be slower than gas phase reactions. Gremyachkin[31] had suggested in his modeling work that for small particles, the reaction could be kinetics controlled. One main disadvantage of the diffusion controlled combustion assumption is that the precise species and temperature profiles cannot be calculated. The approach taken was to include the full kinetics and examine the limiting factors in the combustion process. In this paper, four oxidizer mixtures, namely, O_2-Ar, O_2-N_2, CO_2-Ar, H_2O-Ar are considered.

The kinetic mechanism in the model consists of surface reactions and gas phase reactions for the formation of the aluminum sub-oxides. The aluminum sub-oxides later react and condense to form liquid aluminum oxide. The path to condensation consists of two steps; a homogeneous gas phase reaction, followed by homogeneous condensation. The combustion mechanism accounts for the first kinetic step of the two-step process, while the second step is described with the condensation model in the next subsection.

Unfortunately, the kinetic data in the literature for all the required aluminum reactions is not very accurate for the temperature regime considered. Reliable kinetic data for the Al-O_2 reactions has been published only recently.[63] As for the Al-CO_2 reaction, even though the data have been obtained only for the temperature range of 300°-1900° K, the lack of other kinetic data has forced the extrapolation of the available data to higher temperature ranges.[77] These data had been used by King[67] for his modeling work. The kinetic data for the Al-H_2O reaction has been obtained only for the 298°-1174° K temperature range, but as in the Al-CO_2 reaction, the lack of data has forced the extrapolation of the available data to

the 2000°-4000° K temperature range.[77] There has been little investigation done into the probable condensation paths for the aluminum oxide formation when the oxidizers are CO_2 or H_2O. Hence, the condensation paths in the presence of CO_2 and H_2O oxidizers are taken to be the same as the pure O_2 oxidizer case.[77]

Surface reactions:

$$Al_{(l)} \rightarrow Al_{(g)} \quad \text{(R1)}$$

$$Al_{(l)} + AlO_{(g)} \xrightarrow{k_2} Al_2O_{(g)} \quad \text{(R2)}$$

Gas phase reactions:

$$Al_{(g)} + O_2 \xrightarrow{k_3} AlO + O \quad \text{(R3)}$$

$$k_3 = 9.76 \times 10^{13} \exp(-80/T)\ cm^3 mol^{-1} s^{-1}$$

$$AlO + O_2 \xrightarrow{k_4} AlO_2 + O \quad \text{(R4)}$$

$$k_4 = 4.63 \times 10^{14} \exp(-10008/T)\ cm^3 mol^{-1} s^{-1}$$

$$Al + CO_2 \xrightarrow{k_5} AlO + CO \quad \text{(R5)}$$

$$k_5 = 2.5 \times 10^{-13} T^{0.5} \exp(-1030/T) + 1.4 \times 10^{-9} T^{0.5} \exp(-14000/T)$$

$$Al + H_2O \xrightarrow{k_6} AlO + H_2 \quad \text{(R6)}$$

$$k_6 = (1.9 \pm 1.5) \times 10^{-12} \exp(-(442.87 \pm 221.44)/T) + (1.6 \pm 0.7) \times 10^{-10} \exp(-(2868.6 \pm 452.94)/T)$$

$$O + O + M \xleftrightarrow{k_7} O_2 + M \quad \text{(R7)}$$

$$k_7 = 6.17 \times 10^{15} \times T^{-0.5} \exp(0/T)$$

$$O + N_2 \xrightarrow{k_8} NO + N \quad \text{(R8)}$$

$$k_8 = 1.80 \times 10^{12} \exp(-38345.14/T)$$

$$N + O_2 \xrightarrow{k_9} NO + O \quad \text{(R9)}$$

$$k_9 = 6.40 \times 10^{09} \exp(-3125.26/T)$$

Dissociation reaction:

$$Al_2O_{3(l)} \xrightarrow{k_{10}} 2AlO + \frac{1}{2} O_2 \quad \text{(R10)}$$

Condensation:

$$2AlO + \frac{1}{2} O_2 \xrightarrow{k_{11}} Al_2O_{3(l)} \quad \text{(R11)}$$

$$2AlO + CO_2 \xrightarrow{k_{12}} Al_2O_{3(l)} + CO \quad \text{(R12)}$$

$$2AlO + H_2O \xrightarrow{k_{13}} Al_2O_{3(l)} + H_2 \quad \text{(R13)}$$

$$Al_2O + O_2 \xrightarrow{k_{14}} Al_2O_{3(l)} \quad \text{(R14)}$$

$$Al_2O + 2CO_2 \xrightarrow{k_{15}} Al_2O_{3(l)} + 2CO \quad \text{(R15)}$$

$$Al_2O + 2H_2O \xrightarrow{k_{16}} Al_2O_{3(l)} + 2H_2 \quad \text{(R16)}$$

$$AlO_2 + AlO_2 \xrightarrow{k_{17}} Al_2O_{3(l)} + \frac{1}{2} O_2 \quad \text{(R17)}$$

The rate of the first reaction, which represents the rate of vaporization of the molten aluminum, is given by the boundary condition (Equation 34, see below). While the rate of vaporization depends on the surface temperature (i.e., boiling point of the aluminum metal), the boiling point depends on the pressure of the system. The vast majority of earlier models have assumed that the temperature of the aluminum particle is fixed at the boiling point of aluminum at atmospheric pressure. The relation between the boiling point and the vapor pressure of the aluminum vapor has been expressed in this model as

$$T_{\text{boil}} = (\text{P}/7.6673\times 10^{-43})^{1/12.266} \tag{7}$$

The dissociation temperature is a function of the pressure of the system too. It is expressed as a function of the partial pressure of the aluminum sub-oxides and aluminum oxides using the Clausius-Clayperon equation. The relation between the dissociation temperature, which is the upper limit of the flame temperature, and the vapor pressure of aluminum oxide is

$$T_{\text{flame}} = 1/(0.000250501-14.132\times 10^{-6}\times \ln(\text{P})) \tag{8}$$

The second reaction is assumed to be a diffusion controlled surface reaction. Gaseous Al_2O gets transported away from the particle after the reaction. All the gas phase reactions except (R5) and (R6) have been represented by fundamental reactions. As explained previously, the lack of sufficient reliable kinetic data has been a limiting factor in the number of equations considered. Reaction (R10) is not represented by a rate expression, instead the dissociation reaction keeps dissociation temperature of aluminum oxide as the upper limit of the flame temperature. The following equation is solved to determine $\dot{\omega}_{dAlO}$ to keep $T_{ij}=T_{\text{flame}}$.

$$f_{ij}(T_{ij},\dot{\omega}_{dAlO}) - T_{flame} = 0 \tag{9}$$

The reactions (R11)-(R17) are the first step of the condensation. It is assumed that

$$k_{11} = k_{12} = k_{13} = k_{14} = k_{15} = k_{16} = k_{17} = \dot{\omega}_{cond}\,. \tag{10}$$

Condensation Model

Experimental studies have shown the presence of aluminum sub-oxides near the particle surface[63] during the combustion process and the main end product to be liquid aluminum oxide. The aluminum sub-oxides must thus be consumed in the production of liquid aluminum oxide. A simple kinetic mechanism alone cannot be considered for the production of aluminum oxide from aluminum sub-oxides due to the thermodynamics. Thermodynamically, the heat of the reaction of aluminum sub-oxides to form liquid aluminum oxide is sufficient to cause the dissociation of the newly formed liquid aluminum oxide. Hence, there must be a mechanism beyond a simple kinetic mechanism to form the liquid aluminum oxide. This is simulated in the Liang & Beckstead condensation model. The condensation model consists of a two-step process as shown below.

$$aC_m + bC_n \xrightarrow{k_r} Al_2O_{3(g)} \xrightarrow{\gamma_{cm}} Al_2O_{3(l)} \tag{R18}$$

The first step is a chemical reaction that gives gaseous aluminum oxide (R11-R17). It can be described by an Arrhenius expression. The second step is a condensation process of gaseous aluminum oxide to liquid aluminum oxide. It may be noted here that gaseous aluminum oxide has not been observed experimentally and that liquid aluminum oxide would be expected to dissociate before vaporizing. However, from calculations, it has been observed that the rate of the condensation step is far greater than that of the kinetic step. The gaseous aluminum oxide can thus be considered as an intermediate product with a very short life time. The intermediate product nature of gaseous aluminum oxide, combined with the complexity of the combustion process, warrants some assumptions and the condensation model seems to be reasonable. The number of reactions considered for the first step have been limited by the kinetic data availability in the literature.

Homogeneous condensation is assumed to occur for the second step. Homogeneous condensation refers to condensation processes where the nuclei formation for condensation occurs randomly due to interactions between the constituents in the vapor phase and is not catalyzed by surfaces, ions or impurity molecules. Homogeneous nucleation can occur only in supersaturated vapors.[78] It can be described by classical homogeneous nucleation theory.[78] A nuclei can grow into a droplet if it can attain a size greater than a critical radius. The critical radius is calculated as the radius for which the ΔG is a maximum for a given supersaturation.[78]

For the first reaction step, the rate expression is

$$\dot{\omega}_1 = k_r C_m^a C_n^b \tag{11}$$

For the second condensation step, the rate expression is

$$\dot{\omega}_2 = C_c r_{con} \tag{12}$$

where r_{con} is the nucleation rate. The rate of the nucleation is calculated as the rate of sticking of molecules impinging upon the nuclei with critical radius. From homogeneous nucleation theory,[78]

$$r_{con} = (\alpha_i^* P_\infty / kT)(2\sigma/\pi m)^{\frac{1}{2}} (m/\rho) n_1 \exp\left[-\frac{16\pi\sigma^3 v^2}{3k^3T^3(\ln S)^2}\right] \tag{13}$$

where m is the mass of a molecule, ρ is the liquid density, n_i^* is the number of critical size clusters per unit volume, ν is the volume per molecule in the liquid state.

The total rate for the two-step condensation process is

$$\dot{\omega}_{cond} = \frac{1}{\frac{1}{\dot{\omega}_1} + \frac{1}{\dot{\omega}_2}} = \frac{C_c k_r r_{con} C_m^a C_n^b}{k_r C_m^a C_n^b + C_c r_{con}} = \frac{r_{con} C_m^a C_n^b}{\frac{C_m^a C_n^b}{C_c} + \frac{r_{con}}{k_r}} \tag{14}$$

Next it is assumed in the model that the denominator in Equation (14) does not change significantly during the condensation. So the equation reduces to

$$\dot{\omega}_{cond} = K r_{con} C_m^a C_n^b \tag{15}$$

where K becomes an empirical constant.

In Equation (14) the supersaturation S of the vapor phase has a large effect on the condensation process. It has been experimentally observed[78] that in homogeneous nucleation, for nuclei to start forming, the supersaturation should exceed a critical level and that the condensation rate increases more than proportionally with an increase in supersaturation. For a typical condensation process

$$S = \frac{p}{p_\infty} \tag{16}$$

where p is the partial pressure of the vapor in system and p_∞ is the vapor pressure of the condensed phase.

In the aluminum combustion process, p is zero since aluminum oxide dissociates before it vaporizes. So Equation (16) cannot be used in Equation (15). Instead Equation (17) has been used to determine S.

$$S = 1 + \frac{\sum_i p_i}{p_{Al}} \tag{17}$$

where p_i is the partial pressure of species i, and i= AlO , AlO_2, Al_2O. The partial pressure term in (16) is thus substituted for by the sum of the partial pressures of the aluminum sub-oxides and aluminum, the

components of aluminum oxide dissociation. It is difficult to define a vapor pressure for aluminum oxide, due to the dissociation processes. The vapor pressure term in (16) is taken to be the partial pressure of aluminum in (8). In the condensation process, liquid aluminum oxide is formed from aluminum sub-oxides, which in turn are formed from aluminum. Hence, the more the partial pressure of aluminum, the lesser is the concentration of aluminum sub-oxides, and in turn the lesser is the concentration of liquid aluminum oxide, which should imply a lesser supersaturation according to (13). The assumption for vapor pressure of aluminum oxide in (17) can thus be explained qualitatively. Many of the previous models have assumed condensation to take place in an infinitely thin zone[2,31] or on the particle surface.[41,79] This model has relaxed that assumption and the condensation depends on factors such as species concentration, supersaturation, temperature, and hence on the position.

It has been assumed that the oxide deposits uniformly on the particle surface and migrates to the downstream side to coalesce into an oxide cap. It has been observed experimentally that the oxide does not dissolve in the metal, but rather stays on the surface.[45] The coalescence has been observed experimentally[45] and has been explained by the difference in the surface tension of the molten metal and oxide. The hollow nature of oxide caps is not accounted for in the model. Whether any reactions occur between the oxide cap and the metal on the particle surface has not been established clearly experimentally. Hence, that possibility has not been considered here.

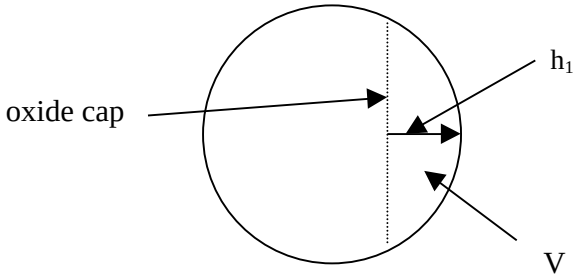

Figure 11. Model of oxide deposition on the aluminum particle surface.

The deposition height h_1 shown in Figure 11, can be described by the equation

$$h_1^3 - 3Rh_1^2 + \frac{3V}{\pi} = 0 \tag{18}$$

where V is the volume of the cap calculated from the $Al_2O_{3(l)}$ diffusion to the particle surface. It may be noted that the radius and mass of the particle changes with time due to the aluminum vaporization and due to the aluminum oxide deposition, thus causing a change in u_∞, the particle velocity with time. According to the model, the oxide cap inhibits aluminum vaporization from the portion of the sphere it covers. This is because the oxide has almost twice the density of the metal and so the metal cannot diffuse through the oxide. The particle surface temperature does not exceed the dissociation temperature of the oxide but is above the melting point of the oxide. So the oxide exists in a molten state throughout. The model does not account for any physical processes that may be involved in the initial bonding of the diffusing oxide to the particle surface. Also, the time required for the diffusion of the oxide to the particle surface is assumed to be the limiting factor in the deposition. In other words, the deposition is assumed to be diffusion controlled.

General Mathematical Model

The general form of the governing equation can be written as

$$\frac{\partial \rho\varphi}{\partial t} + \quad (\rho V\varphi) = \quad (\Gamma_\varphi \quad \varphi) + S_\varphi \tag{19}$$

In spherical coordinates,

$$(\rho V\varphi) = \frac{1}{r^2}\frac{\partial}{\partial r}(\rho r^2 u_r \varphi) + \frac{1}{r\sin\theta}\frac{\partial}{\partial \theta}(\rho u_\theta \sin\theta\varphi) \tag{20}$$

$$(\Gamma_\varphi \quad \varphi) = \frac{1}{r^2}\frac{\partial}{\partial r}(\Gamma_\varphi r^2 \frac{\partial \varphi}{\partial r}) + \frac{1}{r^2}\frac{1}{\sin\theta}\frac{\partial}{\partial \theta}(\Gamma_\varphi \sin\theta \frac{\partial \varphi}{\partial \theta}) \tag{21}$$

For the continuity equation,

$$\Phi=1, \Gamma_\Phi = 0 \text{ and } S_\Phi = 0 \tag{22}$$

For the r-direction momentum equation,

$$\Phi = u_r, \ \Gamma_\Phi = \mu \text{ and}$$

$$S_\Phi = -\frac{\partial p}{\partial r} + \frac{\rho u_\theta^2}{r} + \frac{1}{r^2}\frac{\partial}{\partial r}\left(r^2 \mu \frac{\partial u_r}{\partial r}\right) + \frac{1}{\sin\theta}\frac{\partial}{\partial \theta}\left(\mu \sin\theta \frac{\partial}{\partial r}\left(\frac{u_\theta}{r}\right)\right) -$$

$$\mu\left(\frac{2}{r^2}\frac{\partial u_\theta}{\partial \theta} + \frac{4u_r}{r^2} + \frac{2u_\theta \cot\theta}{r^2}\right) + \frac{4}{3r}\mu\left(\quad \vec{V}\right) - \frac{2}{3r^2}\frac{\partial}{\partial r}\left[r^2 \mu\left(\quad \vec{V}\right)\right] \tag{23}$$

For the θ-direction momentum equation,

$$\Phi = u_\theta, \ \Gamma_\Phi = \mu \text{ and}$$

$$S_\Phi = -\frac{1}{r}\frac{\partial p}{\partial \theta} + \frac{\rho u_r u_\theta}{r} + \frac{1}{r^2 \sin\theta}\frac{\partial}{\partial \theta}\left(\mu \sin\theta \frac{\partial u_\theta}{\partial \theta}\right) + \frac{1}{r^2 \sin\theta}\frac{\partial}{\partial \theta}\left(2\mu u_r \sin\theta\right) -$$

$$\frac{1}{r^2}\frac{\partial}{\partial r}\left(r\mu u_\theta\right) + \frac{1}{r^2}\frac{\partial}{\partial r}\left(r\mu \frac{\partial u_r}{\partial \theta}\right) - \frac{1}{r\sin\theta}\frac{\partial}{\partial \theta}\left(\frac{2}{3}\mu \sin\theta\left(\quad \vec{V}\right)\right) + \mu\frac{\partial}{\partial r}\left(\frac{u_\theta}{r}\right)$$

$$+ \frac{\mu}{r^2}\frac{\partial u_r}{\partial \theta} - \frac{\mu \cot\theta}{r}\left(2\left(\frac{u_r}{r}\right) + \frac{u_\theta \cot\theta}{r}\right) - \frac{2}{3}\left(\quad \vec{V}\right) \tag{24}$$

For the species conservation equations,

$$\Phi = Y_i, \ \Gamma_\Phi = \rho D_i \quad (i \neq Al_2O_{3(l)}), \ \Gamma_{Al_2O_{3(l)}} = \frac{\nu}{\sigma_A} \text{ and } S_\Phi = \dot{\omega}_i \tag{25}$$

where Y_i is the mass fraction of species i, σ_A is the Schmidt number (with $\sigma_A = 0.5$)

and i= $Al, AlO, Al_2O, AlO_2, O_2, O, Al_2O_{3(l)}, Y_{N_2} = 1 - \sum_{i \neq N_2} Y_i$

To ensure a balance of the mass, the calculated diffusion velocities, $\vec{V}_i = -\frac{D}{Y_i} \quad Y_i$, are corrected by a uniform velocity vector to keep

$$\sum Y_i \vec{V}_i = 0 \tag{26}$$

For the energy equation,

$$\Phi = T, \quad \left(\Gamma_\Phi \quad \Phi\right) = \frac{1}{C_{pm}} \quad (k \quad T) \text{ and}$$

$$S_\Phi = \frac{1}{C_{pm}}\left[\frac{Dp}{Dt} - \sum_i^N h_i \dot{\omega}_i - \sum_i^N \rho Y_i \vec{V}_i \quad (C_{pi} \quad T) + \sum_i^N (\rho Y_i \vec{V}_i \quad \vec{f}_i)\right] \tag{27}$$

where $\vec{f}_i$ is the body force of unit mass of species i.

Introducing non-dimensional quantities, the non-dimensional form of equation (19) is

$$\frac{\partial(R\rho^*\varphi)}{\partial t^*} + \quad (\rho^* V^* \varphi) = \frac{1}{R\rho_\infty u_{ref} R_o} \quad (\Gamma_\varphi \quad \varphi) + \frac{RR_o}{u_{ref}\rho_\infty} S_\varphi + \frac{\partial(r^*\rho^*\varphi)}{\partial r^*}\frac{dR}{dt} \tag{28}$$

Boundary Conditions

(1) Inlet condition:

The model considers the particle falling downward under the effect of gravity after being released from an initial position. The particle thus encounters the oxidizer at a velocity $u_\infty(t)$ in a coordinate system that considers the particle to be stationary. The inlet conditions are the conditions at a distance of 60 particle radii from the center of the particle. the inlet conditions are not affected by the combustion process.

$$u_\theta^* = \sin\theta\,,\ u_r^* = -\cos\theta\,, T^* = 1,\ u_\infty = u_\infty(t) \tag{29}$$

For O_2-N_2 oxidizer, $Y_{0_2} = 0.233,\ Y_{N_2} = 0.767\ Y_i = 0.(i \neq O_2, N_2)$

For O_2-Ar oxidizer, $Y_{0_2} = 0.233,\ Y_{Ar} = 0.767\ Y_i = 0.(i \neq O_2, Ar)$

For CO_2-Ar oxidizer, $Y_{C0_2} = 0.233,\ Y_{Ar} = 0.767\ Y_i = 0.(i \neq CO_2, Ar)$

For H_2O-Ar oxidizer, $Y_{H_20} = 0.233,\ Y_{Ar} = 0.767\ Y_i = 0.(i \neq H_2O, Ar)$

The inlet velocity $u_\infty(t)$ is governed by

$$m_p \frac{du_\infty}{dt} = m_p g - C_D \frac{\rho_\infty}{2} u_\infty^2 A - \int_s \rho u_i^2 \vec{n}\ \vec{i}_\infty ds \tag{30}$$

The first term on the right hand side represents the gravity term; the second term represents the drag term, where $C_D = 24/\mathrm{R}$. Creeping flow around the particle is assumed, since the Reynolds number is low due to the small size of the particle. The last term on the right hand side is integration on the particle surface to consider the contribution of the evaporation to the particle movement.

(2) Outlet condition:

$$\frac{\partial\varphi^*}{\partial r} = 0 \tag{31}$$

(3) Symmetrical condition:

$$\frac{\partial\varphi^*}{\partial\theta} = 0,\ u_\theta = 0\,,\ (\theta = 0, \pi) \tag{32}$$

The symmetrical condition has been assumed for simplicity.

(4) Particle surface interface condition:

Energy balance:

$$k_g \left.\frac{\partial T_g}{\partial r}\right|_s - Q_2 \dot{m}_{AlO}\big|_s + Q_{dep} + Q_{rad} = \dot{m}_{vap}\Delta h_{vap} \tag{33}$$

The physical interpretation of this equation is that the heat required for the evaporation of the droplet and the reaction (R2) is provided by the heat feed back from conduction of heat from gases near the particle surface, radiation heat flux from the flame and the heat due to deposition of condensed aluminum oxide. The radiation term consists of the difference between the radiation flux to the particle and the radiation flux from the particle. The shape factors are not considered. There is no evaporation in the area covered by the oxide cap. The oxide cap is at a temperature far greater than the particle surface. This causes energy Q_{dep} to be transferred to the particle for evaporation from the depositing oxide cap. The temperature of the particle surface has an upper limit of the boiling point of aluminum, at which point the evaporation starts to occur. The Stefan flow is assumed not to affect the heat transfer to the particle surface.

$$\dot{m}_{vap} + \dot{m}_{AlO}\Big|_s \frac{M_{Al_2O}}{M_{AlO}} = \rho_s u_{r_s} \tag{34}$$

According to (34), the bulk flow from the particle outwards is due to the flow of Al and Al_2O. It may be noted that the two surface reactions (R1) and (R2) result only in the products Al and Al_2O, which leave the surface and move outwards as they are both gases. It is interesting to analyze the direction of bulk velocity away from the surface. While the direction of the bulk velocity away from the surface is determined from the conservation equations and boundary conditions, it may be noted that one of the main factors influencing the bulk velocity, apart from the inlet velocity of the oxidizer is the velocity of the products. In a typical metal combustion, the volumetric rate of the products is lesser than that of the reactants. Even though the formation of an oxide cap in aluminum combustion results in diffusion of the products towards the particle, in a combustion experiment with a stationary aluminum particle, the bulk velocity in the infinity- flame front zone may be expected to be towards the particle, while the bulk velocity in the flame front- particle zone may be expected to be towards the flame front. The presence of an input velocity may change the direction of the bulk velocity, but the surface condition remains the same and (34) still holds.

Species balance:

$$Y_{AlO} = 0 \tag{35}$$

This relation is because reaction (R2) is assumed to be diffusion controlled so that no AlO should be found at the particle surface.

$$Y_{Al(g)} = \frac{p_{Al}}{p}\frac{M_{Al}}{\bar{M}} \tag{36}$$

This relation assumes the ideal gas law, which is valid at such high temperatures.

$$\rho D_{Al_2O}\frac{\partial Y_{Al_2O}}{\partial r}\Big|_s + \dot{m}_{AlO}\Big|_s \frac{M_{Al_2O}}{M_{AlO}} = \rho u_r Y_{Al_2O}\Big|_s \tag{37}$$

Equation (3728) implies that the net rate of Al_2O transport, which is equal to the rate of Al_2O diffusing outwards, is equal to the rate of production of Al_2O. Any other flux of Al_2O diffusing will be countered by the bulk flow at the surface. In other words, there is no accumulation of Al_2O on the surface and whatever Al_2O is produced on the surface is transported from the surface, which is to be expected since Al_2O is a gas.

$$\rho D_i \frac{\partial Y_i}{\partial r}\Big|_s = \rho u_r Y_i\Big|_s \qquad i \neq Al, Al_2O, Al_2O_3 \tag{38}$$

Equation (38) implies that the net flux of all the other species other than Al_2O, Al_2O_3 and Al at the surface is zero, or in other words there is no accumulation of the other species on the surface, which is to be expected since all those species are gaseous.

$$T = {}^{34860}\!/_{[12.537 - \ln(p_{Al})]} \qquad \text{(King}^{67}\text{)} \tag{39}$$

This relation is used to determine the partial pressure of aluminum at the surface, from the particle surface temperature.

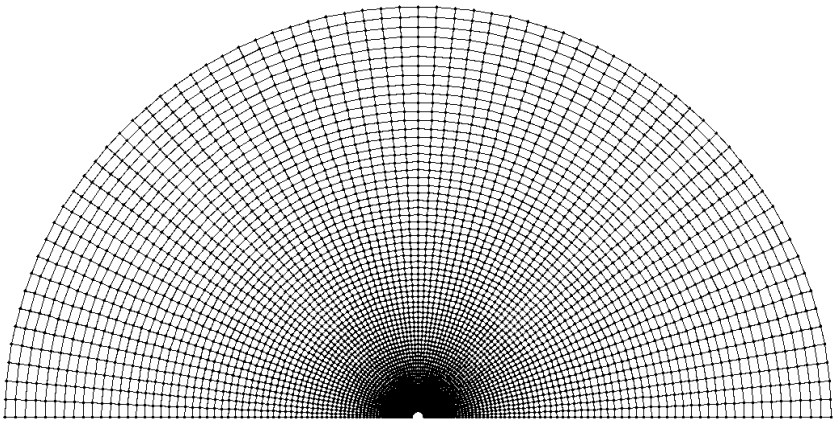

Figure 12 Computation domain for the numerical method.

The fully implicit SIMPLER[80] algorithm is used to solve the partial differential equations in which QUICK scheme is used. A staggered grid system is used where the velocities are defined at the control volume surface and scalar quantities are defined at the center of the control volume. The grid is uniform in the θ direction with 71 nodes. Non-uniform grids are used in the r-direction in order to improve the accuracy. There are 80 nodes in the r-direction extending upto 60 times the particle radius. The smallest distance between grids in the r-direction is near the particle surface and is about 0.0001 r_o. The gas phase grid used in this study is shown in Figure 12.

The role in constructing a non-uniform grid QUICK scheme is to always use two upwind nodes and one downwind node as shown in Figures 13 and 14. For example, consider the control volume i below

when $u_e > 0$,

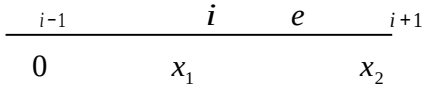

Figure 13. Construction of QUICK scheme when $u_e > 0$

and

$$\varphi_e = \varphi_i + \left[\frac{(x_1 - x_2)^2}{4x_1x_2}\varphi_{i-1} + \frac{x_2 - 3x_1}{4x_1}\varphi_i + \frac{x_1 + x_2}{4x_2}\varphi_{i+1}\right] \quad (40)$$

when $u_e < 0$,

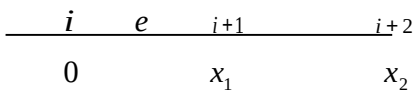

Figure 14. Construction of QUICK scheme when $u_e < 0$

and $$\varphi_e = \varphi_{i+1} + \left[-\frac{x_1(2x_2 - x_1)}{4x_1x_2}\varphi_i + \frac{2x_2 - 3x_1}{4(x_1 - x_2)}\varphi_{i+1} + \frac{x_1^2}{4x_2(x_1 - x_2)}\varphi_{i+2} \right] \quad (41)$$

Modeling Results and Discussion

To check the validity of the unsteady simulation, an unsteady flow passing a sphere was simulated, calculating the wake development as a function of time. The results were very reasonable, and the final wake length is in good agreement with available experimental data.[81]

Model calculations have been made for a variety of conditions, to help validate the model and to explore the effects of different gases and conditions. An analysis of the temperature profiles in Figure 15 shows that the flame temperature for the three oxidizers, O_2, H_2O and CO_2 are different, which is to be expected when thermodynamics are considered. The flame temperature of CO_2 is lesser than the dissociation temperature of aluminum oxide, because the enthalpy of the reaction and hence the heat released is not sufficient to raise the flame temperature to the dissociation temperature.[62] The flame temperature is equal to the dissociation temperature for both the cases of the O_2 and H_2O, which implies that some of the product liquid aluminum oxide gets dissociated to limit the flame temperature.

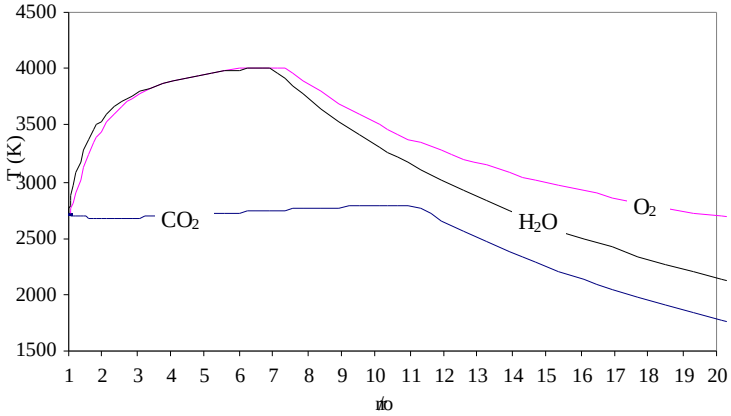

Figure 15 Temperature profiles for 21% O_2/Ar, 21% CO_2/Ar, and 21% H_2O/Ar cases, T_{amb}=300 K, P=1 atm.

Figures 16-18 show the 2-dimensional view of the calculated temperature profile around a burning particle for the three environments corresponding to the results in Figure 7.

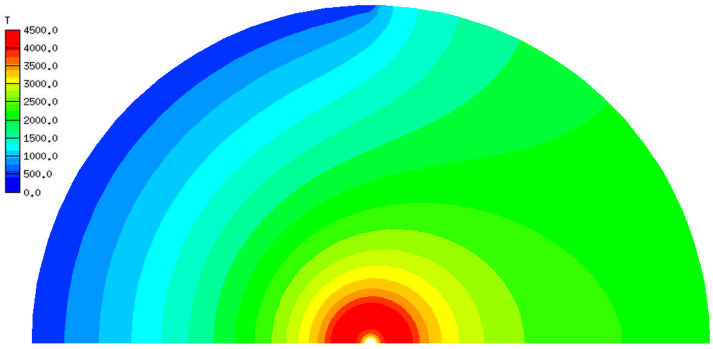

Figure 16. Predicted temperature distribution for aluminum particle combustion in 21%O_2/Ar, T_{amb}=300K, P= 1 atm, d=230 microns.

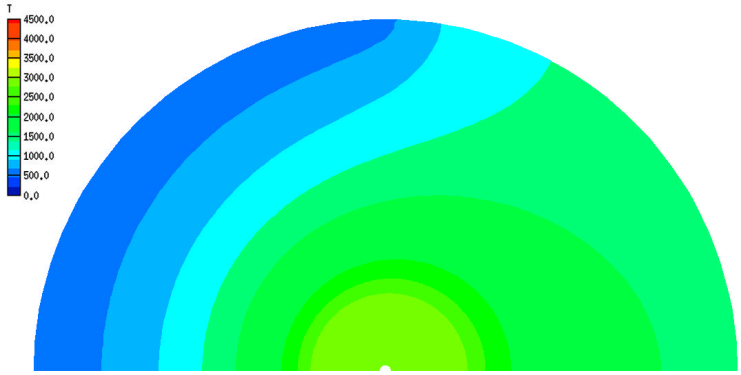

Figure 17. Predicted temperature distribution for aluminum particle combustion in 21%CO_2/Ar, T_{amb}=300K, P=1 atm, d=230 microns.

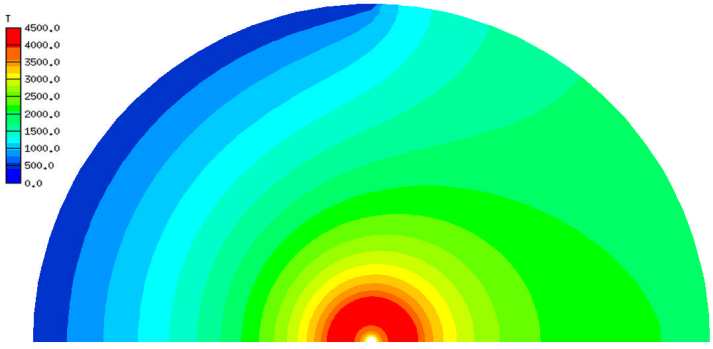

Figure 18 Predicted temperature distribution for aluminum particle combustion in 21%H_2O/Ar, T_{amb}=300K, P=1 atm, d=230 microns.

The flame zone for aluminum combustion includes the reaction zone and the condensation zone, both of which release a large amount of energy. The flame zone can be discerned from the plateau in the temperature profile, wherein the temperature is maintained at the dissociation temperature of the aluminum oxide. The flame zone location has been predicted to be farthest from the particle for the case of the CO_2 oxidizer, and closest to the particle in the case of the H_2O oxidizer. Turns et al observed in their experiments that the flame zone was closer to the particle surface in the presence of H_2O than without H_2O. One of the reasons attributable to this behavior is the value of the diffusivities. While H_2O has the highest diffusivity in Ar, CO_2 has the lowest diffusivity of the three oxidizers in Ar. The higher diffusivity results in the oxidizer diffusing relatively faster towards the particle than the aluminum diffusing outwards. In all the three cases, the aluminum diffuses through an almost similar mixture, dominated by argon. However, this argument holds good only when the convection is comparable to the diffusion, which is true for the present case, wherein the velocity has been assumed to be at a steady at 0.001m/sec. Another effect to be considered would be the evaporation rate of aluminum. In the case of CO_2-Ar, since the flame temperature is comparatively low, the evaporation rate should be lesser and hence the stoichiometric amount of fuel and oxidizer should be obtained at a relatively closer distance to the particle surface due to this effect. It may be noted that for diffusion flames, the flame zone is the region where the fuel and oxidizer are in stoichiometric amounts.

It may be seen from Figures 19-24 that the combustion resembles a diffusion flame for the considered cases, since the region in which the reactants coexist is very small. The fuel and the oxidizer are seen to coexist at the edge of the flame zone in all the cases. This implies that the condensation tends to concentrate in a region closer to the particle surface than the reaction zone, and the condensation results in a large flame zone. Many of the models have assumed infinite kinetics[2,66,65] and hence a diffusion controlled model. The predictions of this model, namely the little coexistence of the aluminum and oxidizer for the oxidizers O_2, CO_2, H_2O, gives validity to that assumption. The conclusion drawn above assumes that the kinetics are well represented in the model. An observation can be made, about the assumption of condensation occurring in the reaction zone in some models, from the flame zone predicted in the model. As stated earlier, condensation tends to concentrate in a region a little bit closer to the particle surface than the reaction zone. Hence, based on the predictions of this model for the oxidizers and conditions studied, it can be concluded that the models that assumed the condensation to occur in the reaction zone were more accurate than the models that took the condensation to occur on the particle surface.

The 2-dimensional pictures are a view of the upper half of the particle shown in Figure.10. The 2-dimensional pictures show the effect of the oxide cap and convection on the distortion of the temperature profiles. The low temperature on the left side of the figures is a combined effect of the convection, which makes the gases flow from left to right, and the oxide cap, which accumulates on the left side. An interesting observation is that on the upper side of the falling particle, the temperature is around 1000° - 1250°K at a distance of 60 radii from the particle. The oxidizer concentration is also not equal to the ambient concentration even at a distance of 20 r_o. This tends to point to the need for group combustion studies. In a rocket motor, there is a good chance of particle spacing in the order of 60 r_0.

The main combustion product is seen to be Al_2O_3. It can be seen that some of the oxide diffuses outwards, which is the oxide smoke. This model does not attempt to determine the size of the oxide smoke, which is expected to be a function of the condensation. The concentration of the aluminum sub-oxides is negligible at distances far from the particle surface, which is to be expected considering their fast condensation and other kinetic reactions. AlO is seen to be main aluminum sub-oxide produced in the flame zone. The concentration of the argon at the particle surface is non-zero, as the argon passes through the flame zone without any reaction. Although any possible reaction between some of the products like H_2, CO & oxide cap with the aluminum has not been considered in this model due to the constraint of kinetic data availability, those reactions could have a role in the fragmentation and jetting of aluminum particles, which has been observed experimentally.[47,82]

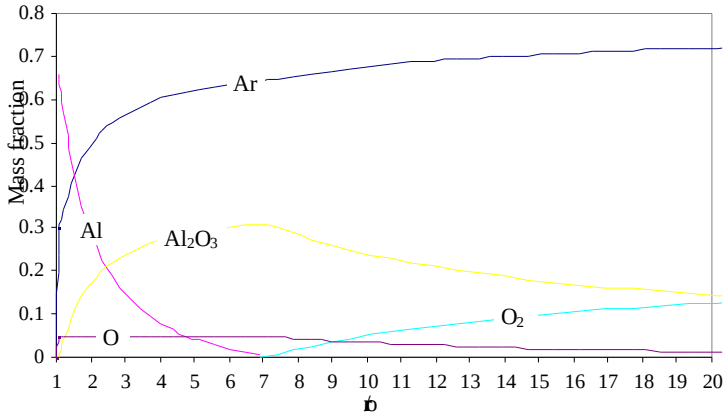

Figure 19. Major species mass fraction for 21%O_2/Ar, T_{amb}=300 K, P= 1 atm.

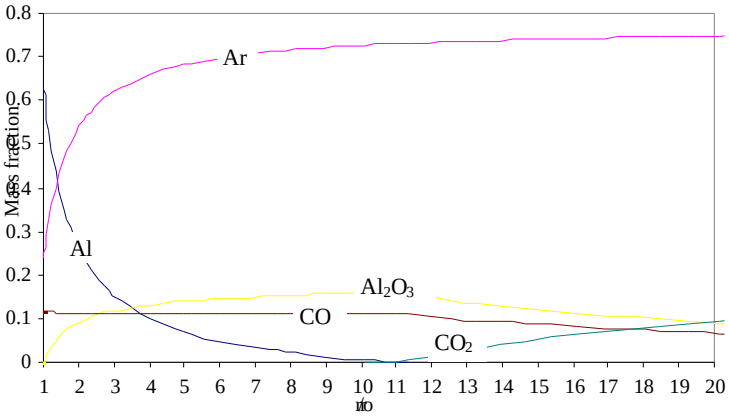

Figure 20. Major species mass fraction for 21%CO_2/Ar, T_{amb}=300 K, P= 1 atm.

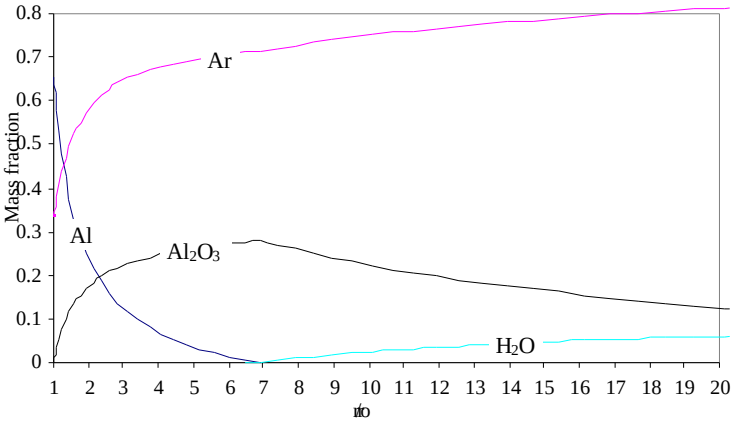

Figure 21. Major species mass fraction for 21%H_2O/Ar, T_{amb}=300K, P=1 atm.

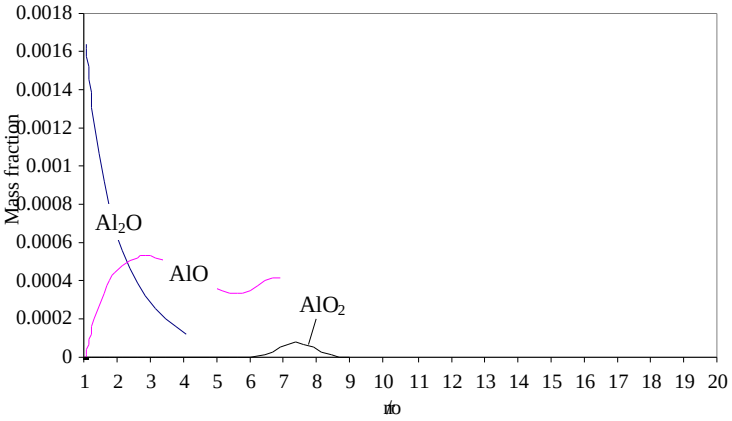

Figure 22. Minor species mass fraction for 21%O_2/Ar, T_{amb}=300 K, P= 1 atm.

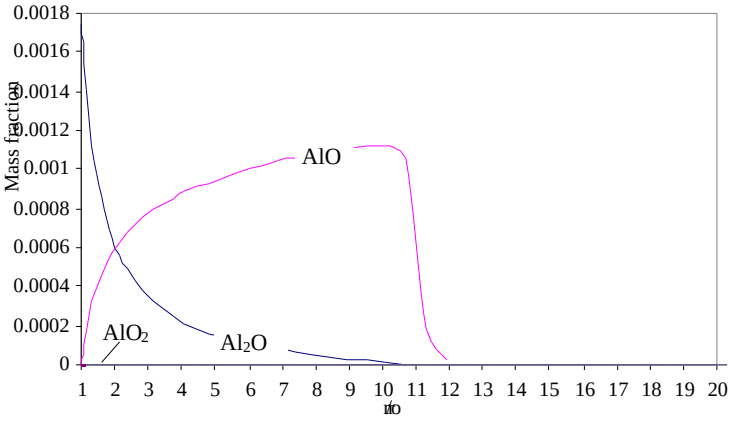

Figure 23. Minor species mass fraction for 21%CO_2/Ar, T_{amb}=300 K, P= 1 atm.

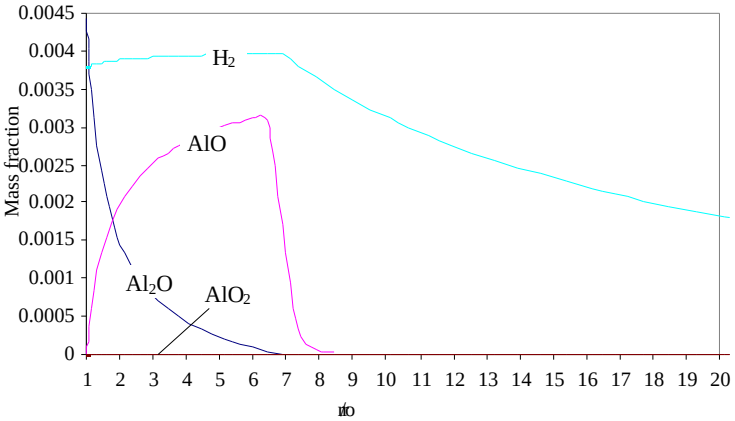

Figure 24. Minor species mass fraction for 21%H_2O/Ar, T_{amb}=300K, P=1 atm.

The effect of pressure on aluminum combustion, which has not been addressed in a lot of experimental and modeling efforts, needs to be given priority considering the rocket motor conditions. Figures 25 and 18 show the calculated temperature distributions for a particle burning at 1 atm and 65 atm pressure respectively. The gas composition used in the calculations was the same as that by Davis[35], so that the results of the model could be compared with the experimental data. The first observation which can be made is the difference in overall temperatures. The surface and flame temperatures are higher for the high pressure case than for the low pressure case. The flame temperature is ~400K higher at 65 atm. This is reasonable because the aluminum and aluminum oxide boiling (dissociation for aluminum oxide) points have increased with ambient pressure. This increase in flame temperature is a very important concept which has not been treated by most investigators. The second observation which may be drawn from these figures is that the flame zone was calculated to be more narrow and closer to the surface at high pressure than at low pressure. Brzustowski and Glassman[2] showed experimentally that in metal combustion an increase in pressure is accompanied by an approach of the flame front toward the particle surface. This agrees with the calculations illustrated in Figures 17 and 18.

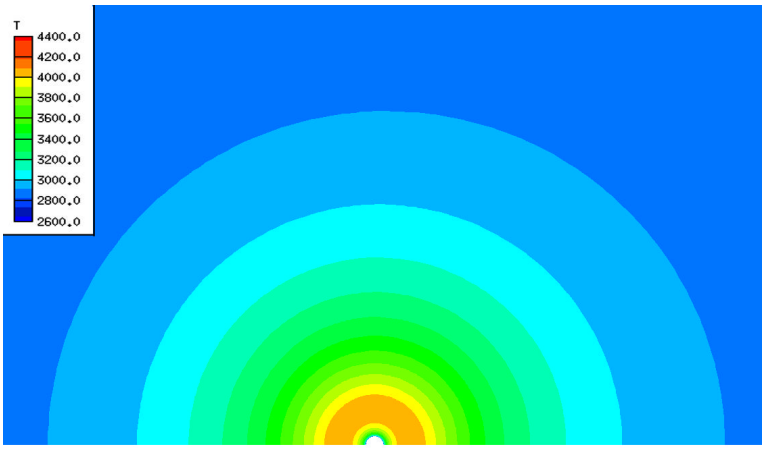

Figure 25. Predicted T(K) distribution in 44.4% H_2O, 11.4% O_2, 13.9% CO_2, 10.1% N_2, 20.2% HCl, T_{amb}=2600 K, and P= 1 atm.

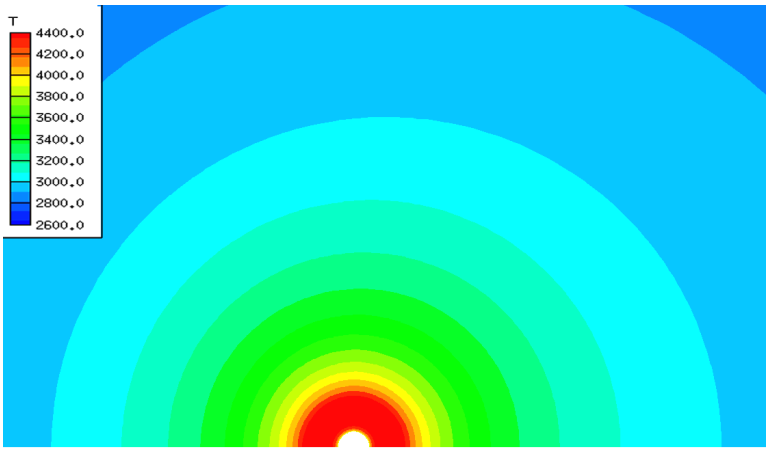

Figure 26. Predicted T(K) distribution in 44.4% H_2O, 11.4% O_2, 13.9% CO_2, 10.1% N_2, 20.2% HCl, T_{amb}=2600 K, and P= 65 atm.

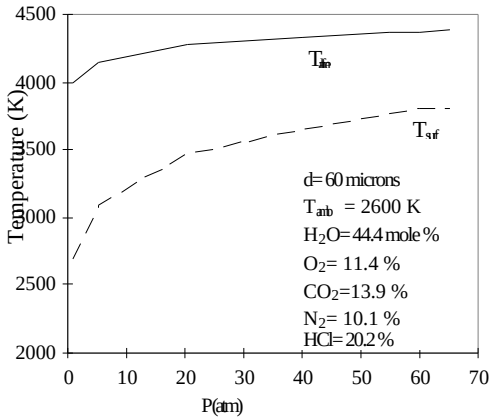

Figure 27. Predicted particle surface and temperatures as pressure is varied.

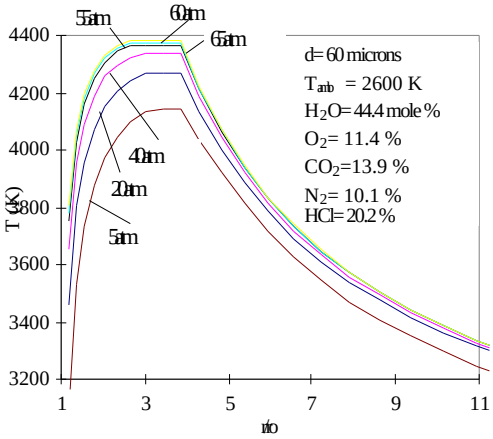

Figure 28. Predicted temperature profiles vs. flame non-dimensional radius for various pressures.

Figure 27 shows the predicted dependence of surface temperature and flame temperature on pressure. Notice that there is a gradual increase in surface and flame temperatures as the pressure is increased. The case of one atm and 65 atm has been demonstrated already in Figures 25 and 26. Figures 27 and 28, however, show the trend over the entire pressure range studied. Figure 28 puts this into a spacial perspective, showing the distribution of the calculated temperatures from the surface outward. In Figure 28, the predicted temperature profiles vs. non-dimensional radius are shown for the same range of pressures as in Figure 27. It can be seen that the temperature profile of the flame zone is increasing in height as the pressure increases.

It is interesting to compare some of the results from Liang's modified model with recent experimental data. Some of the latest and best experimental measurements of temperature and species distributions around a burning aluminum particle have been performed by Bucher et al.[61,62,63] at Princeton. In one of their experiments, they burned aluminum particles in an O_2/Ar atmosphere and measured the temperature profile extending outward from the particle surface in very small increments. Figure 29 shows a comparison of Bucher's data with the temperature profile calculated by the modified Liang model.[69] Excellent agreement between predictions and measurements was achieved.

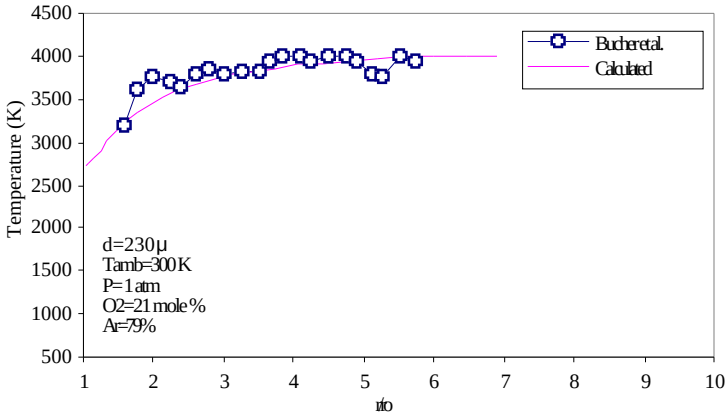

Figure 29. Calculated temperature (K) profile vs. non-dimensional radius compared with experimental data from Bucher et al.

Figure 30 shows the calculated relative AlO concentration profile compared with data from the same experiment. It can be seen that the profiles are very similar, although Bucher et al. observed a peak in AlO concentration at around r/r_o= 2.2, and the calculated peak value is at ~ 3.0. Figure 31 shows a comparison of Bucher's data with a calculated temperature profile for an N_2/O_2 atmosphere, similar to the Ar/O_2 case shown in Figure 29. It must be noted that the dissociation of N_2 was not included earlier in these calculations, hence the disagreement between the earlier calculated values and experiment. However, very recent calculations, which take into account the N_2 dissociation, result in much better agreement between the two as shown in Figure 31. This is a very logical outcome since heat is required to dissociate N_2, thus lowering the calculated temperature of the system. In addition to looking at temperature and species profiles, the burn times calculated by this model were compared against experimental data, as well as against calculated values from the Brooks model.[65] Figure 32 shows several burn times predicted by the modified Liang model, along with calculated burn times from the modified Brooks (analytical) model,[69] as well as experimental data from Hartman[37] and Davis[35] Only a limited number of calculations were performed because of the time required for each calculation (about 12 cpu hours).

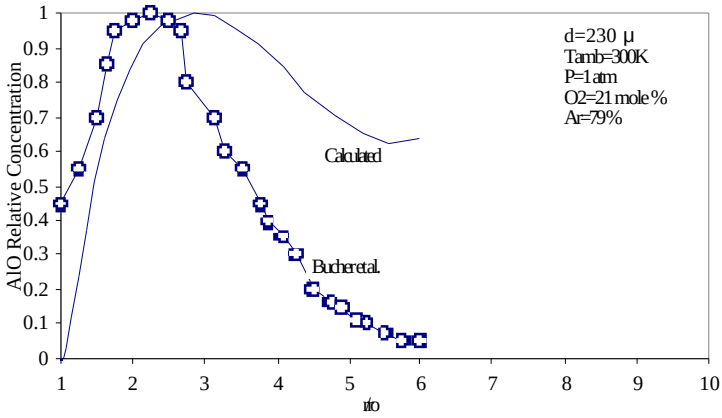

Figure 30. Calculated relative AlO concentration vs. non-dimensional radius compared with experimental data from Bucher et al.

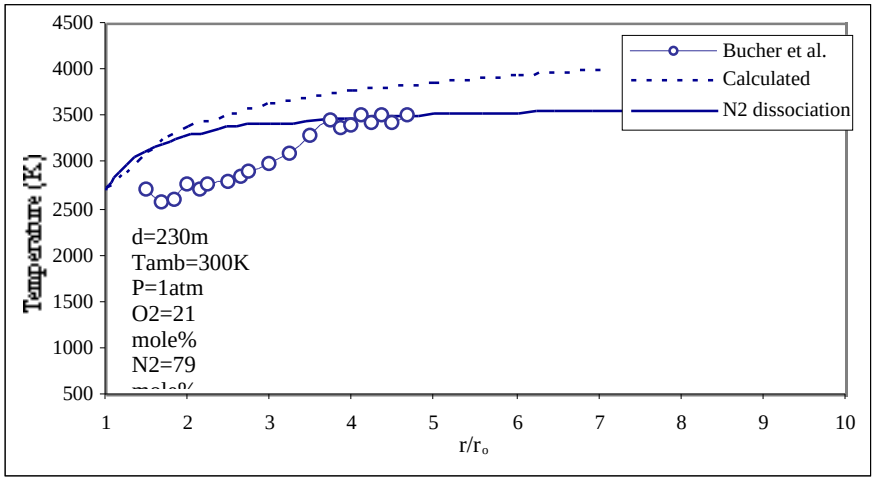

Figure 31. Calculated temperature profile versus non-dimension radius compared with experimental data from Bucher, et al, with N_2 replacing Ar as the inert gas.

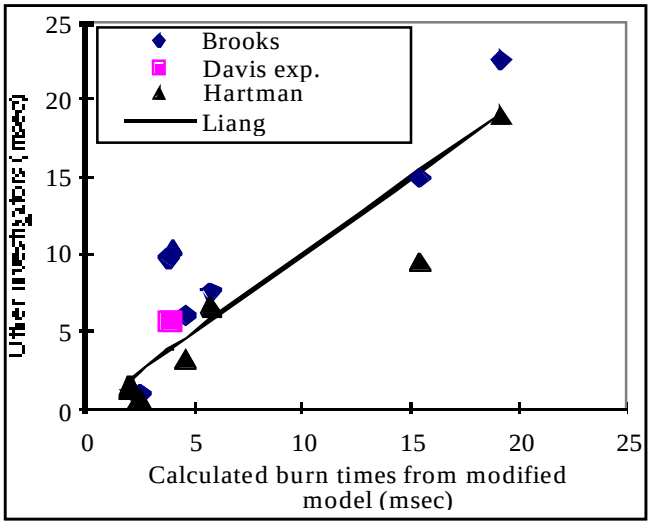

Figure 32. Comparison of burn times calculated by the modified Liang model with calculations from the modified Brooks (analytical) model, and with experimental data from Hartman[37] and Davis. [35]

Since Liang's model is a steady-state calculation, a particle burn time had to be approximated from the calculated steady-state evaporation rate of aluminum. To do this, it was assumed that the steady-state evaporation rate represented the initial rate, and that thereafter the evaporation rate was proportional to the fraction of original aluminum remaining. In addition, when 95 percent of the original aluminum was evaporated, the particle combustion was assumed complete. In this manner, particle burn times were approximated from the steady state calculations, and are shown in Figure 32. As can be seen from this figure, there seems to be reasonable agreement between the calculations of the modified Liang model, the modified Brooks (analytical) model, and experiment

For the analysis of the condensation, dissociation rates and the reaction rates of some of the reactions, the case of aluminum combustion in air has been analyzed. Figure 33 shows the dissociation rate of aluminum oxide. It can be seen that the dissociation occurs exactly in the region where there is a temperature plateau.

The condensation rate of liquid aluminum oxide is shown in Figure 34. We can see the condensation determines the location of the flame and the temperature distribution and occurs very rapidly in a narrow region. Figure 35 shows a plot of the reaction rates of some species in the aluminum combustion process in air. The reaction of aluminum with oxygen is observed to occur only in the narrow flame zone. Between the particle surface and the flame zone the most important species is AlO. AlO is produced in the flame zone and diffuses back to the particle surface reacting with the liquid aluminum to form Al_2O. In the flame zone there are two reactions of species AlO. One is to form AlO_2 and another is the condensation reaction. Figure 35 shows that the formation of AlO_2 is the dominant process. Because of these two reactions, the concentration of AlO at the outer edge of flame goes to zero.

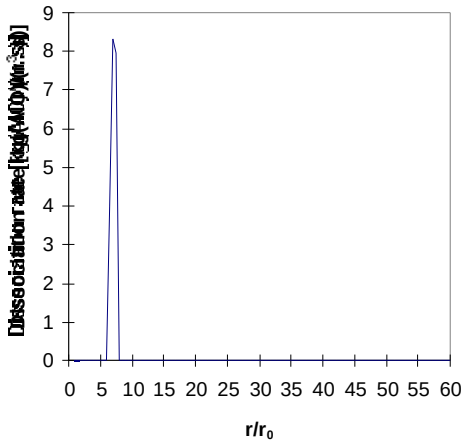

Figure. 33 Dissociation rate of aluminum oxide vs. radial non-dimensional distance

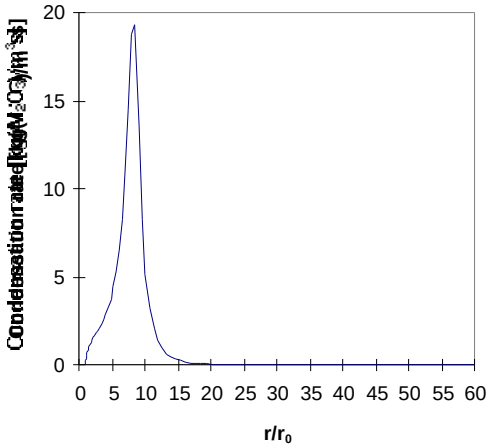

Figure. 34 Condensation rate vs. radial non-dimensional distance

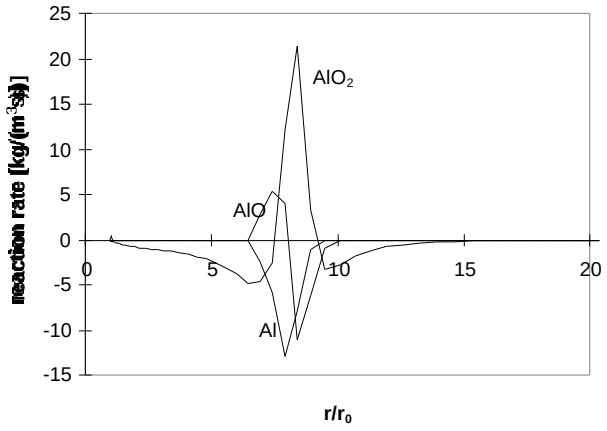

Figure 35. Reaction rate vs. radial non-dimensional distance

The condensation reaction[18] $AlO_2 + AlO \rightarrow Al_2O_{3(l)}$ cannot occur at that location which will let a lot of AlO_2 exist in the final combustion product. Therefore, we assume AlO_2 condenses through reaction (R17) and AlO_2 will be finally condensed. Species $Al_2O_{3(l)}$ is mainly produced in the flame zone and diffuses to the particle surface and deposits on the particle surface. From the results we can see that next to the condensation rate the most important quantity to influence the condensation is the O_2 concentration which is different from the classical condensation process.

For hydrocarbon droplet combustion, the burn time is proportional to the initial diameter raised to the power of 2. For aluminum combustion, the model predicts the burn time to be proportional to the initial diameter raised to the power of 1.2 for small diameters to 1.88 for large diameters. The reason the exponent is lesser than 2 is due to the oxide cap and the convection, which cause the evaporation rate of aluminum to decrease and thus cause the burning time to increase. The oxide cap has another effect of providing energy to the particle surface during deposition, which cancels off some of the effect due to the blockage of the aluminum evaporation due to the oxide cap.

Summary and Conclusions

The combustion characteristics of aluminum combustion have been summarised in an overview of the subject, focusing on the burning time of individual particles. The fundamental concepts that control aluminum combustion are discussed starting with a discussion of the "D^n" law. Combustion data from over ten different sources with almost 400 datum points have been cataloged and correlated. The wide variety of experimental techniques and a lack of standard definitions of the burning time, contribute to the large data scatter observed between different investigators. A thorough evaluation of the data indicates that an exponent on the order of 1.5 to 1.8 correlates the data best, with the value of 1.8 slightly better than 1.5.

There is a rich body of data varying the environmental gases. These data have bee systematically analyzed showing that oxygen is a more powerful oxidizer than water or CO_2. Zenin's data shows that CO_2 is only 20% as efficient as oxygen. Although the data were not conclusive about the precise effect of water, it appears that water is probably about half as effective as oxygen. And about half as effective as CO_2. Interesting studies have been performed using various inert gases while varying the oxygen concentration. There appears to be an effect of the gaseous diffusivity, with the product of the density times the diffusivity. The inference being that smaller gaseous molecules will tend to reduce the burning time. The observed effect of pressure and initial temperature is minimal. Early Russian investigators proposed that pressure has a small effect at low pressure, but no effect above ~20 atm. More recent work seems to verify that trend. The effect of initial temperature is also relatively small with an exponent of -0.2 resulting in a minimization of error.

A proposed equation that can be used to estimate burning times of aluminum particles is (Eqn. 6)

$$t_b = \frac{aD^n}{Xeff\ P^{0.1} T_o^{0.2}}$$

where $Xeff = C_{O2} + 0.6\ C_{H2O} + 0.22\ C_{CO2}$

$a = 0.0244$ for $n = 1.5$ and

$a = 0.00735$ for $n = 1.8$

and pressure is in atmospheres, temperature in K, diameter in μm, and time in msec.

A two-dimensional, unsteady state kinetic-diffusion-vaporization controlled numerical model for aluminum particle combustion is presented. The model solves the conservation equations, while accounting for species generation and destruction with a 15 reaction kinetic mechanism. Two of the major phenomena that differentiate aluminum combustion from hydrocarbon droplet combustion, namely the condensation of the aluminum oxide product and the subsequent deposition of part of the condensed oxide, are accounted for in detail with a sub-model for each phenomenon. The effect of the oxide cap in the distortion of the profiles around the particle has been included in the model.

Parametric calculations were made to examine the flame structure for oxygen, water and carbon dioxide flames. Each of the three calculations was made for a mixture of 21% of the oxidizer mixed with 79% argon, all at one atm. The results show a dramatic difference for the CO_2 case. The flame temperature for the CO_2 case as~2700 K while for both O_2 and water the temperature is ~4000 K. These correspond to the thermodynamic equilibrium for the three oxidizers. There is much less energy in the CO_2 flame. The calculations also indicate that the flame for the CO2 extends further from the surface than either O2 or H2O. The calculated species profiles indicate that the flame corresponds to a diffusion flame as virtually none of the oxidizer penetrates beyond the flame.

The calculated temperature profiles have been compared with recent experimental data by Bucher, et al, showing good agreement between the model and the available data. The modeling results also show that the exponent of the particle diameter dependence of burning time is not a constant and changes from about 1.2 for larger diameter particles to 1.9 for smaller diameter particles. The calculations also indicate that due to the deposition of the aluminum oxide on the particle surface, particle velocity oscillates.

Calculations indicate that both the flame temperature and surface temperature increase with increasing pressure. Between 5 and 60 atm the flame temperature is calculated to increase by approximately 400 K. Calculations were also made for conditions corresponding to what might occur in a solid propellant rocket motor where little oxygen is present, and the principal oxidizers are water and CO_2.

Nomenclature

ρ	density	$\dot{\omega}$	mass flux of ‘species produced’
u	velocity	Δh	latent heat
p	pressure	h	enthalpy
D	diffusivity	R	particle radius
Y	mass fraction	V	velocity vector
T	temperature	C_p	specific heat
M	molecular weight	R_p	instantaneous particle radius
$\dot{m}$	flux	S	supersaturation
k	thermal conductivity		surface tension of a flat liquid surface
m	mass	α_i^*	condensation coefficient
Q	heat flux		

Non-Dimensional variables

$u_r^* = \frac{u_r}{u_\infty}$ non-dimensional radial velocity

$u_\theta^* = \frac{u_\theta}{u_\infty}$	non-dimensional tangential velocity
$t^* = \frac{tu_\infty}{R_0}$	non-dimensional time
$r^* = \frac{r}{R_0}$	non-dimensional radial distance
$\rho^* = \frac{\rho}{\rho_\infty}$	non-dimensional density
$\mu^* = \frac{\mu}{\mu_\infty}$	non-dimensional viscosity
$D_i^* = \frac{D_i}{D_\infty}$	non-dimensional diffusivity
$T^* = \frac{T}{T_\infty}$	non-dimensional temperature
$p^* = \frac{p}{\rho_\infty u_\infty^2}$	non-dimensional pressure

Subscripts

r	radial direction	vap	vaporization
θ	tangential direction	dep	deposition
∞	infinity conditions	0	initial condition
p	particle	i	species
g	gas	m	mean
s	surface		

References

[1] Glassman, I., "Metal Combustion Processes", American Rocket Society Preprint 938-59, New York, 1959.

[2] Brzustowski, T. A. and Glassman I., "Spectroscopic Investigation of Metal Combustion", Heterogeneous Combustion, Academic Press, New York, 1964, pp 41-74.

[3] Pokhil, P. F., Belyayev A. F., Frolov Yu. V, Logachev V. S. and Korotkov A. I., "Combustion of Powdered Metals in Active Media", Nauka, FTD-MT-24-551-73 (English translation), 1972.

[4] Frolov, Yu. V., Pokhil P. F. and Logachev V. S., "Ignition and Combustion of Powdered Aluminum in High-Temperature Gaseous Media and in a Composition of Heterogenous Condensed Systems", *Combustion, Explosion & Shock Waves*, Vol. 8, No. 2, 1972, pp. 168-187

[5] Micheli, P. L. and Schmidt W. G., "Behavior of Aluminum in Solid Rocket Motors", *AFRPL-TR-77-29*, Vol II, Aerojet Solid Propulsion Co., 1977.

[6] Glassman, I., Mellor A. M., Sullivan H. F. and Laurendeau N. M., "A Review of Metal Ignition and Flame Models", AGARD Conference Proceedings No. 52, 1970, pp. 19-1 - 19-30.

[7] Price, E. W., Kraeutle K. J., Prentice J. L., Boggs T. L., Crump J. E. and Zurn D. E., "Behavior of Aluminum in Solid Propellant Combustion", *NWC TP 6120*, Naval Weapons Center, 1982,

[8] Price, E. W., "Combustion of Metalized Propellants", *Fundamentals of Solid-Propellant Combustion*, Volume 90, Progress in Astronautics and Aeronautics, Chapter 14, 1984, pp. 479-514

[9] Pressley, H. M., "Survey of Soviet Work in Aluminum Combustion", *14th JANNAF Combustion Meeting*, III, 1977, pp. 85-104.

[10] Belyaev, A. F., Frolov Yu. V. and Korotkov A. I., "Combustion and Ignition of Particles of Finely Dispersed Aluminum", *Combustion, Explosion & Shock Waves*, Vol. 4, No. 3, 1968, pp. 323-329.

[11] Boreisho, A. S., Ivashchenko A. V. and Shelukhin G. G., "Problem of Determining the Sizes of Burning Metal Particles", *Combustion, Explosion & Shock Waves*, Vol. 11, No. 4, 1975, pp. 659-660.

[12] Arkhipov, V. A., Ermakov, V. A., and Razdobreev, A. A., "Dispersity of Condensed Products of Combustion of an Aluminum Drop," *Combustion, Explosions, & Shock Waves*, Vol. 18, No. 2, pp. 16-19, 1982.

[13] Dreizin, W. L. and Trunov M. A., "Surface Phenomena in Aluminum Combustion", *Combustion and Flame*, Vol. 101, No. 3, 1995, pp. 378-382.

[14] Merzhanov, A. G., Grigorjev Yu. M. and Gal'chenko Yu. A., "Aluminum Ignition", *Combustion and Flame*, Vol. 29, 1977, pp. 1-14.

[15] Breiter, A. L., Mal'tsev V. M. and Popov E. I., "Models of Metal Ignition", *Combustion, Explosion and Shock Waves*, Vol. 13, No. 4, 1977, pp. pp 475-484.

[16] Ermakov, V. A., Razdobreev A. A., Skorik A. I., Pozdeev V. V. and Smolyakov S. S., "Temperature of Aluminum Particles at the Time of Ignition and Combustion", *Combustion, Explosion and Shock Waves*, Vol. 18, No. 2, 1982, pp. pp 256-257.

[17] Lokenbakh, A. K., Zaporina N. A., Knipele A. Z., Strod V. V. and Lepin L. K., "Effects of Heating Conditions on the Agglomeration of Aluminum Powder in Air", *Combustion, Explosion & Shock Waves*, Vol. 21, No. 1, 1985, pp. 73-82.

[18] Boiko, V. M., Lotov V. V. and Papyrin A. N., "Ignition of Gas Suspensions of Metallic Powders in Reflected Shock Waves", *Combustion, Explosion & Shock Waves*, Vol. 25, No. 2, 1989, pp. 67-74.

[19] Rozenband, V. I. and Vaganova N. I., "A Strength Model of Heterogeneous Ignition of Metal Particles", *Combustion and Flame*, 88, 1992, pp. 113-118.

[20] Rozenband, V. I., Afanas'eva L. F., Lebedeva V. A. and Chernenko E. V., "Activation of Ignition of Aluminum and its Mixtures with Oxides by Chromium Chloride", *Combustion, Explosions and Shock Waves*, 26, No. 5, 1990, pp. 13-15.

[21] Fedorov, B. N., Plechov Yu. L. and Timokhin E. M., "Particle Size of Aluminum Oxide Particles in the Combustion Products of Condensed Substances", *Combustion, Explosion & Shock Waves*, Vol. 18, No. 1, 1982, pp. 22-27.

[22] Gostintev, Yu. A., Lazarev V. V. and Frolov Yu. V., "Calculation of Critical Combustion Conditions for Metal with High-Velocity Heating by a Stream of Oxidizing Agent", *Combustion, Explosion & Shock Waves* , Vol. 22, No. 3, 1986, pp. 10-14.

[23] Gremyachkin V.M., "Theory of Ignition of Metallic Particles", *Combustion, Explosion & Shock Waves*, Vol. 19, No 3, 1983, pp. 259-262.

[24] Arutyunyan, A. B., Kharatyan S. L. and Merzhanov A. G., "Theory of Metal Particle Ignition I. Ignition of Metal Particles in the Formation of Solid Solutions", *Combustion, Explosion & Shock Waves*, Vol. 15, No. 3, 1979, pp. 16-22.

[25] Gurevich, M. A., Ozerov E. S. and Yurinov A. A., "Effect of an Oxide Film on the Inflammation Characteristics of Aluminum", *Combustion, Explosion & Shock Waves*, Vol. 14, No. 4, 1978, pp. 448-451.

[26] Bezprozvannykh, V. A., Ermakov V. A. and Razdobreev A. A., "Induction Period for the Heating of Metal Particles by Continuous Laser Radiation", *Combustion, Explosion & Shock Waves*, 28, 6, 1992, pp. 60-63.

[27] Kovalev, O. B., "Adiabatic Method in the Thermal Theory of Ignition of Metal Particles in Gases", *Combustion, Explosions and Shock Waves*, Vol. 30, No. 5, 1994, pp. 29-33.

[28] Medvedev, A. E., Fedorov A. V. and Fomin V. M., "Mathematical Modeling of Metal Particle Ignition in the High-Temperature Flow Behind a Shock", *Combustion, Explosion & Shock Waves*, Vol. 18, No. 3, 1982, pp. 261-265.

[29] Kudryavtsev, V. M., Sukhov A. V., Voronetskii A. V. and Shapara A. P., "High-Pressure Combustion of Metals (Three-Zone Model)", *Combustion, Explosion & Shock Waves*, Vol. 15, No. 6, 1979, pp. 731-737.

[30] Gremyachkin, V. M., Istratov A. G. and Leipunskii O. I., "Effect of Immersion in a Flow on Metal-Drop Combustion", *Combustion, Explosion & Shock Waves*, Vol. 15, No. 1, 1979, pp. 32-36.

[31] Gremyachkin, V. M., Istratov A. G. and Leipunskii O. I., "Model for the Combustion of Metal Droplets", *Combustion, Explosion & Shock Waves*, Vol. 11, No. 3, 1975, pp. 313-318.

[32] Babuk, V. A., Belov V. P. and Shelukhin G. G., "Combustion of Aluminum Particles in Composite Condensed Systems Under Low and High Pressures", *Combustion, Explosion & Shock Waves*, Vol. 17, No. 3, 1981, pp. 26-31.

[33] Friedman, R. and Macek A., "Combustion Studies of Single Aluminum Particles", *Ninth Symposium (International) on Combustion*, 1963, pp. 703-709.

[34] Friedman, R. and Macek A., "Ignition and Combustion of Aluminum Particles in Hot Ambient Gases", *Combustion and Flame*, 6, 1962, pp. 9-19.

[35] Davis, A., "Solid Propellants: The Combustion of Particles of Metal Ingredients", *Combustion and Flame*, Vol. 7, 1963, pp. pp 359-367.

[36] Macek, A., "Fundamentals of Combustion of Single Aluminum and Beryllium Particles", *Eleventh Symposium (International) on Combustion*, 1967, pp. 203-217.

[37] Hartman, K. O., "Ignition and Combustion of Aluminum Particles in Propellant Flame Gases", *8th JANNAF Combustion Mtg.*, Vol. 1, 1971, pp. pp 1-24.

[38] Wilson, R. P. and Williams F. A., "Experimental Study of the Combustion of Single Aluminum Particles in O_2/Ar", *Thirteenth Symposium (International) on Combustion*, The Combustion Institute, Pittsburgh, PA, 1971, pp. 833-845.

[39] Prentice, J. L., "Combustion of Laser-Ignited Aluminum Droplets in Wet and Dry Oxidizers", AIAA 12th Aerospace Sciences Meeting, AIAA Paper No. 74-146; see also "Aluminum Droplet Combustion: Rates and Mechanisms in Wet and Dry Oxidizers", NWC TP 5569, 1974.

[40] Wong, S. C. and Turns S. R., "Ignition of Aluminum Slurry Droplets", *Combust. Sci. and Tech.*, 52, 1987, pp..221-242.

[41] Turns, S. R., Wong S. C. and Ryba E., "Combustion of Aluminum-Based Slurry Agglomerates", *Combust. Sci. and Tech.*, Vol. 54, 1987, pp. pp 299-318

[42] Roberts, T. A., Burton R. L. and Krier H., "Ignition and Combustion of Aluminum/Magnesium Alloy Particles in O_2 at High Pressures", *Combustion and Flame*, 92, 1993, pp. 125-143.

[43] Marion, M. Chauveau C. and Gokalp I., "Studies on the Ignition and Burning of Aluminum Particles", *AIAA 95-2861*, 1995,

[44] Marion, M., Chauveau C. and Gokalp I., "Studies on the Ignition and Burning of Aluminum Particles", *Combustion Sci. & Technology*, Vol. 116, 1996, pp. 369-390.

[45] Olsen, S. E. and Beckstead M. W., "Burn Time Measurements of Single Aluminum Particles in Steam and Carbon Dioxide Mixtures", *J. of Propulsion & Power*, Vol. 12, No. 4, 1996, pp. 662-671.

[46] Melcher, J. C., Burton R. L. and Krier H., "Combustion of Aluminum Particles in in Solid Rocket Motor Flows", *36th JANNAF Combustion Meeting*, Vol. I, CPIA # 691, 1999, pp. 249-258.

[47] Dreizin, E. L., "On the Mechanism of Asymmetric Aluminum Particle Combustion", *Combustion & Flame*, Vol. 117, 1999, pp. 841-850.

[48] Dreizin, E. L., "Experimental Study of Aluminum Particle Flame Evolution in Normal and Micro-Gravity", *Combustion & Flame*, Vol. 116, 1999, pp. 323-333.

[49] Zenin, A. A., Kusnezov G. and Kolesnikov V. and Zenin, A. A. Kusnezov G. and Kolesnikov V., "Physics of Aluminum Particle Combustion at Zero-Gravity", AIAA-99-0696, 1999.

[50] Zenin, A. A., Kusnezov G. and Kolesnikov V., "Physics of Aluminum Particle Combustion at Convection", AIAA-2000-0849, 2000.

[51] Burton, R. L., Schneider, D. S., and Krier, H., "Aluminum Particle Combustion in a Pressurized Flow Reactor", *Thirty-Fourth JANNAF Combustion Meeting*, Vol. II, CPIA Pub. No. 662, Laurel, MD, 1997, pp. 287-294.

[52] Melcher, J. C., Burton R. L. and Krier H., "Combustion of Aluminum Particles in in Solid Rocket Motor Flows", *Solid Propellant Chemistry, Combustion and Motor Interior Ballistics*, AIAA Progress in Astronautics and Aeronautics, Vol. 185, 2000.

[53] Bartlett, R. W., Ong J. N., Fassell W. M. and Papp C. A., "Estimating Aluminum Particle Combustion Kinetics", *Combustion and Flame*, Vol. 7, 1963, pp. pp 227-234.

[54] Drew, C. M., Gordon, A. S., and Knipe, R. H., "Study of Quenched Aluminum Particle Combustion," *Heterogeneous Combustion*, AIAA, Progress in Astronautics and Aeronautics Series, Vol. 15, Academic Press, New York, NY, 1964, pp. 17-39.

[55] Gordon, A. S. Drew C. M. Prentice J. L. and Knipe R. H., "Techniques for the Study of the Combustion of Metals", *AIAA Journal*, 6, 4, 1968, pp. 577.

[56] Price, E. W., Christensen, H. C., Knipe, R. H., Drew, C. M., Prentice, J. L., and Gordon, A. S., "Aluminum Particle Combustion Progress Report," NOTS-TP-3916, Naval Ordnance Test Station, China Lake, CA 1966.

[57] Foelsche, R. O., Burton, R. L., and Krier, H., "Ignition and Combustion of Aluminum Particles in $H_2/O_2/N_2$ Combustion Products," *J. of Propulsion and Power*, Vol. 14, No. 6, 1998, pp. 1001-1008.

[58] Brzustowski, T. A. and Glassman, I., "Spectroscopic Investigation of Metal Combustion," pp. 41-73 and "Vapor-Phase Diffusion Flames in the Combustion of Magnesium and Aluminum," *Heterogeneous Combustion*, AIAA, Progress in Astronautics and Aeronautics Series, Vol. 15, Academic Press, New York, 1964,. pp. 75-115,

[59] Drew, C. M., Gordon, A. S., and Knipe, R. H., Kraeutle, K. J., Prentice, J. L., and Price, E. W., "Metal Particle Combustion Progress Report," NWC-TP-4435, Naval Weapons Center, China Lake, CA, 1968.

[60] Prentice, J. L. and Krauetle, K. J., "Metal Particle Combustion Progress Report," NWC-TP-4658, Naval Weapons Center, China Lake, CA, 1969.

[61] Bucher, P., Yetter, R. A., Dryer, F. L., Vicenzi, E. P., Parr, T. P., and Hanson-Parr, D. M., "Observations on Aluminum Particles Burning in Various Oxidizers", *33rd JANNAF Combustion Meeting*, Vol. II, CPIA Pub. No. 653, Laurel, MD, 1996, pp. 449-458

[62] Bucher, P., Yetter, R. A., Dryer, F. L., Parr, T. P., and Hanson-Parr, D. M., "Aluminum Particle Gas-Phase Flame Structure", *34th JANNAF Combustion Meeting*, Vol. II, CPIA Pub. No. 662, 1997, Laurel, MD, pp. 295-305.

[63] Bucher, P., Yetter, R. A., Dryer, F. L., Parr, T. P., and Hanson-Parr, D. M., "PLIF Species and Ratiometric Temperature Measurements of Aluminum Particle Combustion in O_2, CO_2, and N_2O Oxidizers, and Comparison with Model Calculations," *27th Symposium (International) on Combustion*, The Combustion Institute, Pittsburgh, PA, 1998, pp. 2421-2429.

[64] Law, C. K., "A Simplified Theoretical Model for the Vapor-Phase Combustion of Metal Particles, " *Combustion Science and Technology*, Vol. 7, 1973, pp. 197-212.

[65] Brooks, K. P. and Beckstead, M. W., "Dynamics of Aluminum Combustion," *Journal of Propulsion and Power*, Vol. 11, No. 4, 1995, pp. 769-780.

[66] Law, C. K., "A Simplified Theoretical Model for the Vapor-Phase Combustion of Metal Particles, " *Combustion Science and Technology*, Vol. 7, 1973, pp. 197-212.

[67] King, M. K., "Modeling of Single Particle Aluminum Combustion in CO_2/N_2 Atmospheres," *17th (International) on Combustion*, The Combustion Institute, Pittsburgh, PA, 1977, pp. 1317-1328.

[68] Kuo, K. K., *Principles of Combustion*, John-Wiley & Sons, Inc., New York, NY, 1986, pp. 383-385.

[69] Widener, J. F. and Beckstead M. W., "Aluminum Combustion Modeling in Solid Propellant Combustion Products", AIAA 98-3824, 1998.

[70] Liang, Y. and Beckstead, M.W. "Numerical Simulation of Quasi-Steady, Single Aluminum Particle Combustion in Air," AIAA 98-0254, 1998.

[71] Liang, Y., and Beckstead, M.W. "Numerical Simulation of Single Aluminum Particle Combustion in Air," *34th JANNAF Meeting*, 1997, CPIA No. 662, Vol. IV, pp. 197-208.

[72] Liang, Y., and Beckstead, M.W. "Numerical Simulation Of Unsteady, Single Aluminum Particle Combustion In Air", AIAA 98-3825, Cleveland, OH, July 1998

[73] Widener, J.F., Liang, Y and Beckstead, M.W. "Aluminum Combustion Modeling In Solid Propellant Environments", AIAA-98-0449, Los Angeles, CA, June 1999.

[74] Widener, J.F., Liang, Y and Beckstead, M.W. "Aluminum Combustion Modeling In Solid Propellant Environments", *35th JANNAF Combustion Meeting*, 1998, CPIA No 680, Vol I, pp. 577-592.

[75] Kee, R. J., Dixon-lewis, G., Warnatz, J., Coltrin, M. E. and Miller, J. A., "A fortran computer code package for the evaluation of gas-phase multicomponent transport properties", SAND86-8246, 1992.

[76] Bhatia,R. and Sirignano, W.A., "Metal Particle Combustion With Oxide Condensation", Submitted *to Combustion Science & Technology*, 1993.

[77] Widener, J.F. "Computer Modeling Of Aluminum Particle Heat-Up And Combustion Under Rocket Motor Conditions", MS Thesis, Dept. of Chemical Engineering, Brigham Young University, Provo, Utah, 1998.

[78] Zettlemoyer, A. C., *Nucleation*, Marcel Dekker Inc. New York, 1969.

[79] Brooks, K. "Characterization of the Flame and Aluminum Particles in a Rijke Burner", MS Thesis, Dept. of Chemical Engineering, Brigham Young University, Provo, Utah, 1992.

[80] Patankar, S. V., *Numerical Heat Transfer and Fluid Flow*, Hemisphere Publishing Corporation, 1980.

[81] Kalra, T.R. and Uhlherr, P. H. T., Aust. Conf. Hydraul. Fluid Mech. 4th, Melbourne, 1971.

[82] Prentice, J. L. and Nelson,L.S. "Differences between the combustion of Aluminum particles in air and Oxygen-Argon mixtures", *Journal of Electrochemical Society*, Vol.115, 1968, p.809-812.